TÉCNICO LISBOA

Field-Oriented Control for Squirrel-Cage Induction Generators in Pump as Turbines Applications

Samuel Ferreira Amaro

Thesis to obtain the Master of Science Degree in

Electrical and Computer Engineering

Supervisors: Prof. João Filipe Pereira Fernandes
Prof. Paulo José da Costa Branco

Examination Committee

Chairperson: Prof. Célia Maria Santos Cardoso de Jesus
Supervisor: Prof. João Filipe Pereira Fernandes
Member of the Committee: Prof. Luís Guilherme Barbosa Rolim

January 2021

Declaration

I declare that this document is an original work of my own authorship and that it fulfills all the requirements of the Code of Conduct and Good Practices of the Universidade de Lisboa.

Acknowledgments

I would like to thank my parents for their friendship, encouragement and caring over all these years, for always being there for me through thick and thin and without whom this project would not be possible. I would also like to thank my grandparents, aunts, uncles and cousins for their understanding and support throughout all these years.

I would also like to acknowledge my dissertation supervisors Prof. Paulo Branco and Prof. João Fernandes for their insight, support and sharing of knowledge that has made this Thesis possible.

Last but not least, to all my friends and colleagues that helped me grow as a person and were always there for me during the good and bad times in my life. Thank you.

To each and every one of you – Thank you.

Abstract

Pumps operating as turbines (PATs) are a way of improving efficiency in water systems. In these systems, pressure-reducing valves are typically used to regulate the pressure for the water consumers, by dissipating the excess of energy. The PAT is a better alternative to these valves, allowing the recovery of this excess of energy. This solution is especially useful in isolated areas without access to the electrical grid.

In this dissertation it is intended to develop a field-oriented control algorithm that allows control of electrical and mechanical quantities of the generation system and maximizes its efficiency. This algorithm was first developed to control the induction machine speed in stand-alone operation and then changed to control the generator's electromagnetic torque and its shaft's mechanical power. Finally, coupling the PAT to the induction generator, several tests were performed to validate the control algorithms. Since the subject of interest is off-grid operation, it is intended to replace the capacitor banks used in previous works to excite the machine for a three-phase inverter fed by a battery. The maximum efficiency of the generating unit obtained in simulation was $49,8\ \%$ under control conditions.

Keywords

Energy efficiency, Field-Oriented Control, Induction Generator, Loss Minimization, Off-grid Pump as Turbine

Resumo

As bombas operando como turbinas (PATs) são uma forma de melhorar a eficiência dos sistemas de água. Nestes sistemas, válvulas redutoras de pressão são normalmente utilizadas para regular a pressão para os consumidores, dissipando o excesso de energia. A PAT é uma melhor alternativa a essas válvulas, permitindo a recuperação deste excesso de energia. Esta solução é especialmente útil em áreas isoladas sem acesso à rede elétrica.

Nesta dissertação pretende-se desenvolver um algoritmo de controlo por campo orientado que permita o controlo das grandezas elétricas e mecânicas do sistema de geração e maximize a sua eficiência. Este algoritmo foi primeiramente desenvolvido para controlar a velocidade da máquina de indução em operação autónoma e depois alterado para controlar o torque eletromagnético do gerador e a potência mecânica no seu eixo. Por fim, acoplando a PAT ao gerador de indução, diversos testes foram realizados para validar os algoritmos de controlo. Como o interesse é a operação fora da rede, pretende-se substituir os bancos de condensadores utilizados em trabalhos anteriores para excitar a máquina por um inversor trifásico alimentado por uma bateria. A eficiência máxima da unidade geradora obtida em simulação foi de $49,8\ \%$ sob condições de controlo.

Palavras Chave

Bomba como turbina, Controlo por campo orientado, Eficiência energética, Gerador de indução, Minimização de perdas

Contents

List of Figures

List of Tables

Symbols

Induction machine

η_{gen}	induction generator efficiency
w_m	mechanical rotor angular speed
w_r	electrical rotor angular speed
w_s	electrical stator angular speed
θ_s	electrical angle between stator and *d* frame axis
θ_r	electrical angle between rotor and *d* frame axis
θ_{me}	electrical angle between stator and rotor
λ_{ds}	leakage flux of the stator windings in the direct axis
λ_{qs}	leakage flux of the stator windings in the quadrature axis
λ_{dr}	leakage flux of the rotor windings in the direct axis
λ_{qr}	leakage flux of the rotor windings in the quadrature axis
λ_M	mutual flux between stator and rotor
$l_{\sigma s}$	stator leakage inductance
$l_{\sigma r}$	rotor leakage inductance
L_m	mutual inductance between stator and rotor
L_s	total stator inductance
L_r	total rotor inductance
R_s	stator windings resistance
R_r	rotor windings resistance
v_{ds}	stator voltage in the direct axis
v_{qs}	stator voltage in the quadrature axis
v_{dr}	rotor voltage in the direct axis
v_{qr}	rotor voltage in the quadrature axis
i_{ds}	stator current in the direct axis
i_{qs}	stator current in the quadrature axis
i_{dr}	rotor current in the direct axis

i_{qr} rotor current in the quadrature axis

E/f induction machine magnetization level

T_e electromagnetic torque produced by the induction machine

T_L mechanical load torque

T_{losses} friction torque

p pole pairs

V_n nominal three-phase voltage

f_n nominal frequency

I_n nominal stator current

Pump as Turbine (PAT)

η_{PAT} efficiency of the PAT

ρ fluid density

g gravitational acceleration

H head drop

P fluid differential pressure

Q flow rate

P_{hyd} hydraulic power

T_{hyd} hydraulic torque

$T_{mec_{PAT}}$ mechanical torque

1

Introduction

Contents

1.1 Motivation

With the increasing need to avoid depleting natural resources, water supply systems have shown the potential to be used as electrical energy recovery systems. According to [1], it is possible to recover up to 188 MW h/year for 910000 m^3/year of water that is being wasted in Valencia, Spain. In addition to the waste of water, the high required water pressures may also lead to water leakages and pipes damage. Therefore, it is important to recover the energy wasted in water distribution systems. Currently, a solution for that consists of installing pressure-reducing valves, reducing the water pressure and leakages. However, these valves do not allow the energy recovery. By changing these valves for hydraulic machines such as PATs (pumps as turbines), one can, at the same time, prevent such damage and recover electrical energy by coupling it to a generator. This is an especially viable solution for low power applications (< 10 kW) in rural and remote areas without access to an electrical grid but with natural waterfalls or water courses,

This dissertation is conducted within the scope of the international project REDAWN (Reducing Energy Dependency in Atlantic Area Water Networks), with the collaboration of Instituto Superior Técnico (IST) and Universitat Politècnica de València (UPV). This project aims to improve the energy efficiency of water networks through the installation of micro-hydropower technology. Therefore, this work is intended to contribute to this project by analyzing the generator's electrical behavior coupled to a PAT in water distribution systems.

1.2 Objectives

This dissertation intends to contribute to the study of pumps operating as turbines connected to induction generators in off-grid operation by developing a field-oriented control algorithm that will allow control of electrical and mechanical quantities of the generating unit. The works done so far on this subject have used a capacitor bank to supply the necessary reactive power to excite the induction generator since there is no electrical grid access. According to the induction machine operating point, methods to estimate the required capacitance values have been developed and validated in previous works for a range of water pressures and electrical load values.

This thesis studies how the induction generator performance changes under different loads while being fed by a power inverter, instead of being self-excited by a capacitor bank (Figure 1.1). Using a field-oriented-control strategy the torque, mechanical power and speed will be commanded to achieve maximum efficiency by optimizing the machine flux to minimize losses. The present research will then focus on the generator performance under such control conditions when coupled to a single PAT system.

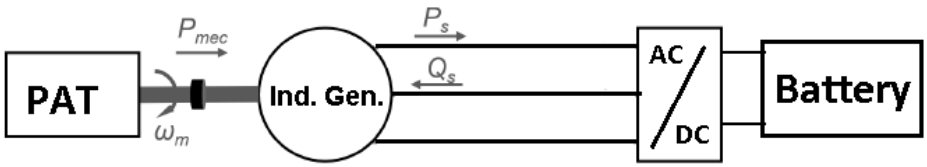

Figure 1.1: Complete generation system with inverter.

1.3 Dissertation structure

This thesis is divided into five chapters.

First, a revision of the state-of-the-art is done in the second chapter. This intends to provide background information on previous research regarding the pump operating as a turbine and the induction generator in off-grid operation.

The third chapter is dedicated to using a previously developed induction machine model to develop the field-oriented control algorithm that allows motor speed control. Speed control is the classical control variable when operating an induction motor. However, the induction machine will be used in a generating unit, where the torque and mechanical power of the system must be controlled.

In chapter four, the control algorithm will be changed to allow mechanical power or electromagnetic torque control, with further tests to evaluate the algorithm performance. Moreover, in this chapter, a loss minimization method for the steady-state operation will be applied. As seen, operating the machine at rated flux is very inefficient at low loads and leads to very high losses. Since the most frequent operating region is at partial load regime, it is of the utmost importance to maximize the generator efficiency for these operation points.

In chapter five, the inclusion of the pump as a turbine in the system is analyzed. A PAT model is described, and tests to evaluate the field-oriented control algorithm performance will be done for the complete generating unit.

In the end, the inclusion of the magnetizing resistance in the machine model is analyzed in chapter six. In the previous chapters, the model used did not include this parameter, which is relevant because it introduces iron losses in the generator. The goal is to analyse its impact on the machine's performance.

2

Literature Review

PATs have demonstrated to be a feasible alternative to conventional turbines for energy recovery systems. Pumps are mass-produced, and there are fewer manufacturers of turbines. Thus, pumps operating in reverse mode can be a solution for generating and recovering energy that otherwise would just be lost. For instance, a PAT technology was tested with a laboratory prototype for a case study of an aqueduct in the city of Merano, Italy [2] [3], in which the authors concluded to be possible to obtain $76\ \%$ of the maximum efficiency of the turbine working in both reverse and direct mode.

In water distribution systems, PATs can replace pressure-reducing valves (used to reduce water pressure and leakages) to recover energy. This kind of energy recovery, complemented by energy storage units, presents a well-known technology and offers a low-cost solution, easy installation, and maintenance [4].

The study's actual interest is the PAT's and generator's off-grid operation for low power applications in rural and remote areas. Capelo [5], but also Williams et al. [6] have identified the induction generator as the most appropriate electrical machine to take into account for energy recovery in water distribution systems. In these situations, factors such as reliability, cost-effectiveness, robustness, and maintenance costs have the same importance as performance and efficiency.

When the electrical grid is present, it supplies the necessary reactive power for the machine excitation. Its absence means that the induction generator has to be excited by some other source. In previous works, the behavior of the PAT-SEIG system was analyzed for a stand-alone application, with capacitor bank to provide the SEIG excitation. These works focused on: a) the impact of the change of SEIG electric parameters on the overall system's efficiency; b) the electro-hydraulic transients on the system due to sudden changes and c) on the behavior of series-connected PAT-SEIG systems.

The work done in [7] has established the required range of capacitance values to excite the generator as a function of its load. Table 2.1 lists the rated values of the generator used in those tests, and the generation system considered is illustrated in Figure 2.1.

Table 2.1: Nominal data of the induction machine.

Siemens Induction Motor 1LA7083-6AA10-Z A23	
Frequency	50 Hz
Voltage	400 V
Current	1.6 A
Output power	550 W
Power factor	0.73
Speed	910 rpm
Pole pairs	3
Stator resistance	23,36 Ω
Rotor resistance	21,12 Ω
Stator and rotor leakage inductance	0,06 H
Inertia	0.011 $\mathrm{kg\,m^2}$

The system's principle of operation is that two different sources feed the generator: the prime mover

(PAT) that supplies the induction generator's shaft with mechanical power and the capacitor bank that supplies the stator with reactive power. For a decrease in the capacitance value, the excitation current supplied to the SEIG will decrease. To supply the same load at rated current, the mechanical power transferred to the shaft has to increase, which increases the rotational speed. On the other hand, if the mechanical power transferred to the shaft decreases, meaning that the rotational speed decreases, the reactive power transferred to the generator must increase so that the load can continue to be supplied at rated current. Now, this is accomplished by increasing the capacitance value.

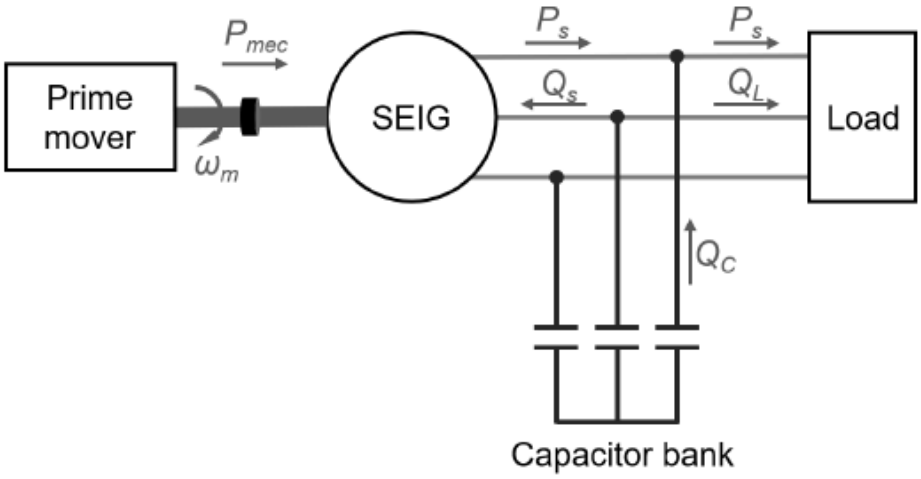

Figure 2.1: Complete generation system with self-excited induction generator.

This work considered that all generator parameters were constant for every operating point. Figure 2.2 shows the generating unit global efficiency obtained under this assumption. The maximum efficiency obtained was $26\ \%$ for a speed of 1200 rpm and a water flow of $4.7\ \mathrm{l\,s^{-1}}$.

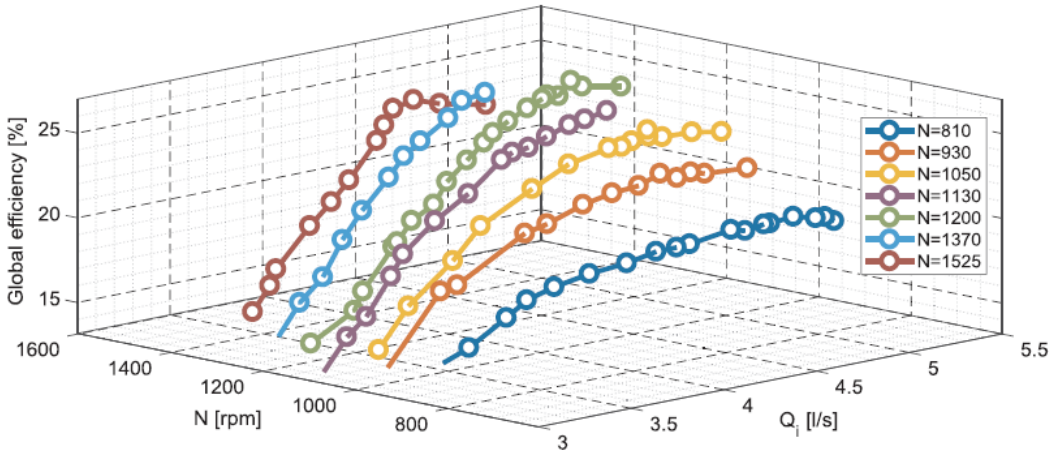

Figure 2.2: Global efficiency as function of flow rate, for different rotational speeds (all generator parameters fixed) obtain in [7].

Optimization of the PAT-SEIG system efficiency when operating under different loads and speeds was studied in [8]. For this purpose, a methodology for tuning the induction machine parameters and thus compute the best capacitance values for different operating points was developed. In this research, it was found that the parameter with the strongest influence in the machine performance is the magnetizing inductance L_m. Specifically, it was verified that the generator's model was more accurate when all electrical parameters of the machine were considered fixed except for L_m. Tests were made to find how L_m changes with the magnetization level E/f. The results obtained are present in Figure 2.3. As for the required capacitance values for the machine excitation, they are present in Figure 2.4 The results obtained in the previous work [7] were included the comparison.

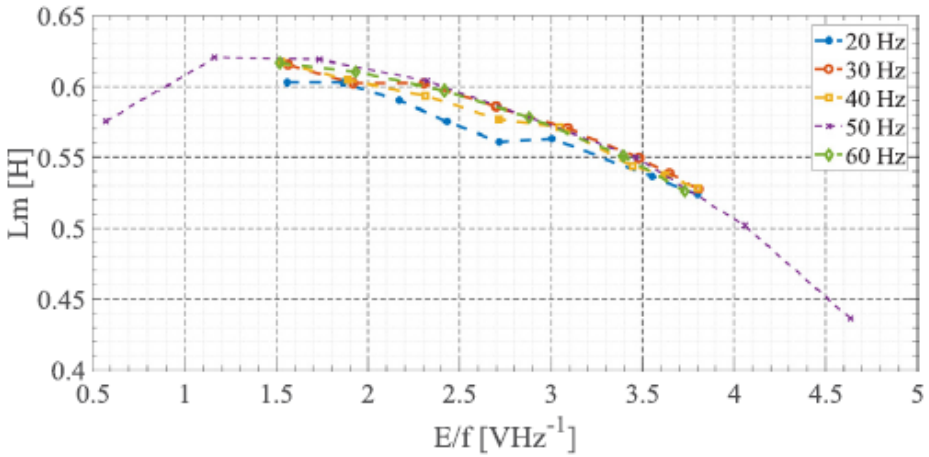

Figure 2.3: Experimental results for the variation of L_m as function of the E/f ratio from [8].

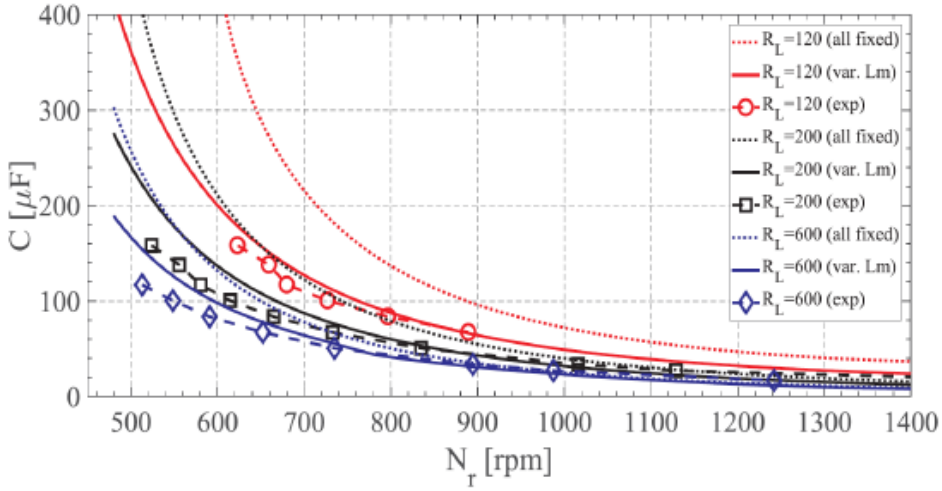

Figure 2.4: Capacitance per phase required for each induction generator rotor speed, for different resistive loads, obtained using the model with only L_m variable [8]. In dotted lines are the results for the analytical model (considering R_m) with all fixed parameters [7].

The evolution of the PAT, generator, and overall efficiencies for various loads while considering a variable L_m are present in Figure 2.5. The overall system efficiency increased from the top $26\ \%$ obtained in [7] to a new maximum of $40\ \%$, showing an improvement of $53\ \%$.

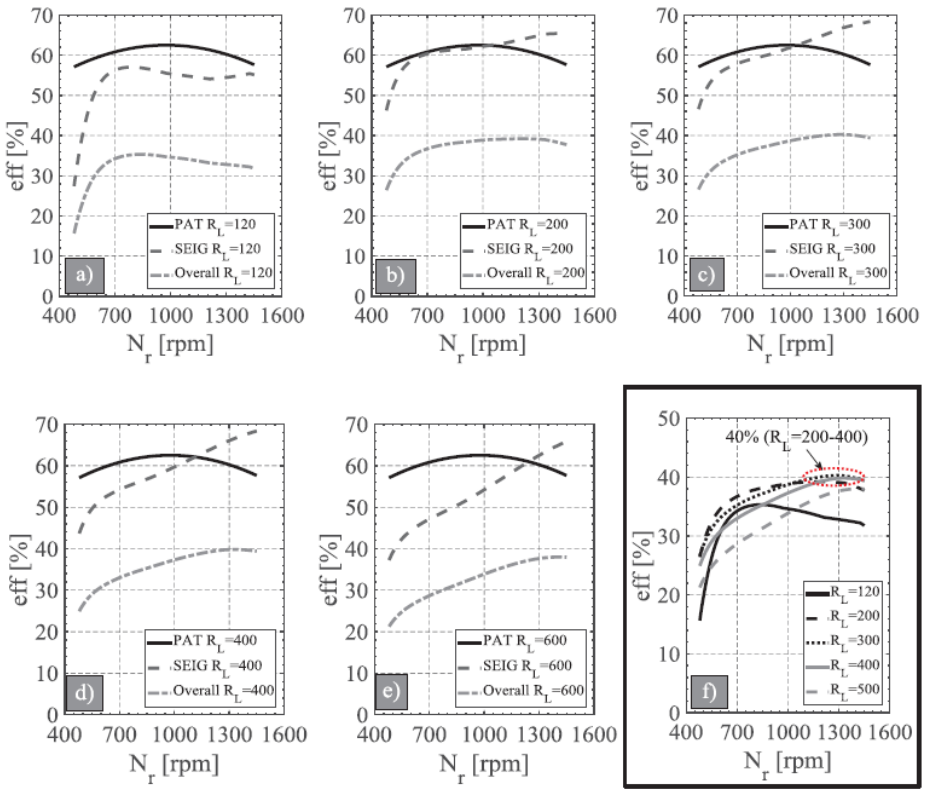

Figure 2.5: Evolution of the SEIG, PAT and overall system efficiencies for different rotor speeds and for the resistive load of RL = [120 (a) 200 (b) 300 (c) 400 (d) 500 (e)] Ω. Comparison between overall efficiencies in (f). [8]

The work done in [9] takes on this research. It aimed to assess the reliability of associating multiple groups of PATs, each connected to a generator and a capacitor bank, to increase the amount of energy recovered. These PAT associations are relevant because it is more cost-effective to invest in several low power pumps than in a single high power pump.

This latest work starts by building a dynamic induction machine model in a rotating magnetic field frame, validating it for the generator's stand-alone operation, both steady-state and transient regimes. The transient response validation was achieved with two different analyses: the first was the dynamic effect of variation in capacitance value; the second was the dynamic effect of variation in load.

Figure 2.6 shows the experimental set-up used in experimental tests. In the tests performed to evaluate the transient response of the induction machine's self-excitation process, a constant resistive load of $R_L = 600\ \Omega$ was used. Figure 2.7 shows stator voltage build-up process while connecting the capacitor bank.

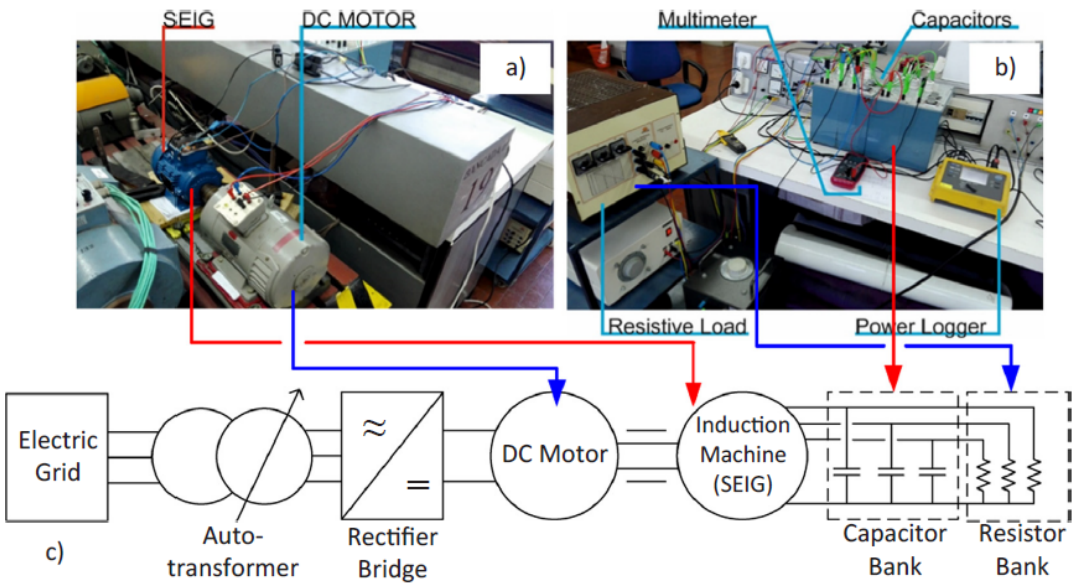

Figure 2.6: Experimental set-up for the measurement of the stator voltage during the transient where the capacitor bank or load were switched between connected and disconnected to the generator. (a) SEIG and DC motor, (b) Capacitor bank, resistive load, power logger and auxiliary measurement equipment, and (c) the electrical diagram of the experimental set-up. [9]

Considering residual magnetism in the rotor, a small voltage starts to be induced at the stator terminals. The capacitors will then be charged, allowing current to flow into the induction machine to produce a stronger magnetic flux. As a consequence, higher voltage is generated at the stator terminals, and so on. This voltage rises gradually until the reactive power produced by the capacitors meet the reactive power required by the induction generator. The most important conclusion regarding changes in the capacitance value is that, when this value decreases, frequency and stator peak voltage increases, as shown in Figure 2.7. As illustrated in Figure 2.4, the minimum capacitance value that can excite the induction machine is related to mechanical speed. As the mechanical angular speed increases, the minimum capacitance value decreases. As speed increases, so does the rotor and stator frequency, increasing the peak voltage.

Table 2.2 confirms the results presented in Figure 2.7. As the capacitance value increases, the mechanical speed decreases, and so do the stator voltages' frequency and magnitude. The model was validated through the experimental work since errors between experimental and model results vary between $1\ \%$ and $4\ \%$.

In the load variation tests, keeping the capacitance value constant, two cases were studied: one with $R_L = 600\Omega$ and another with $R_L = 300\Omega$. The results obtained for stator voltage are represented in Figure 2.8. The two cases started from the same conditions: machine operating at no-load, being fed by certain reactive power and mechanical power. When the load $R_L = 600\ \Omega$ was connected, the machine could supply it. As the load $R_L = 300\ \Omega$ was connected, it demanded more power than the generator

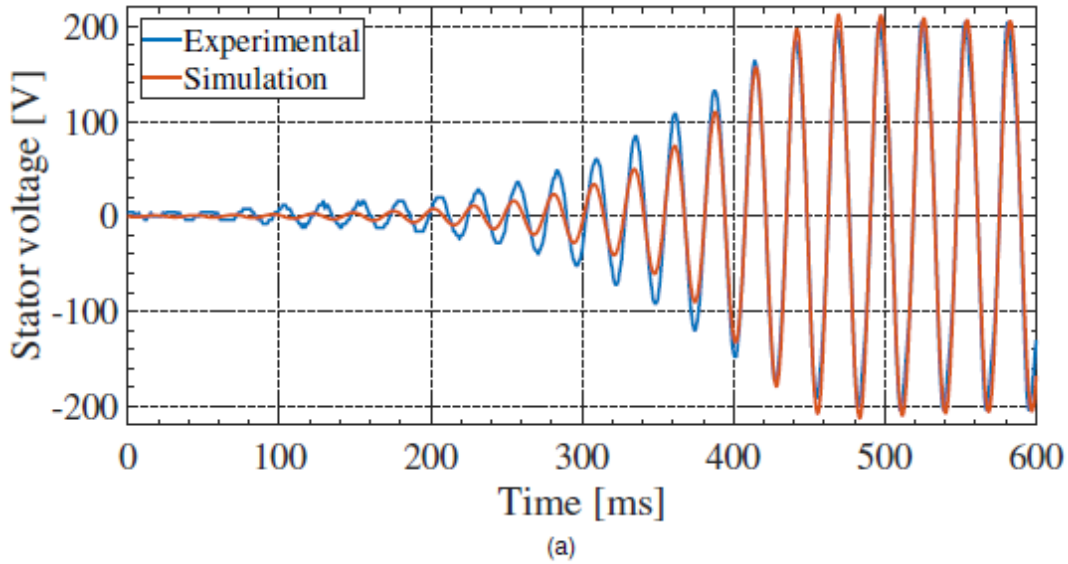

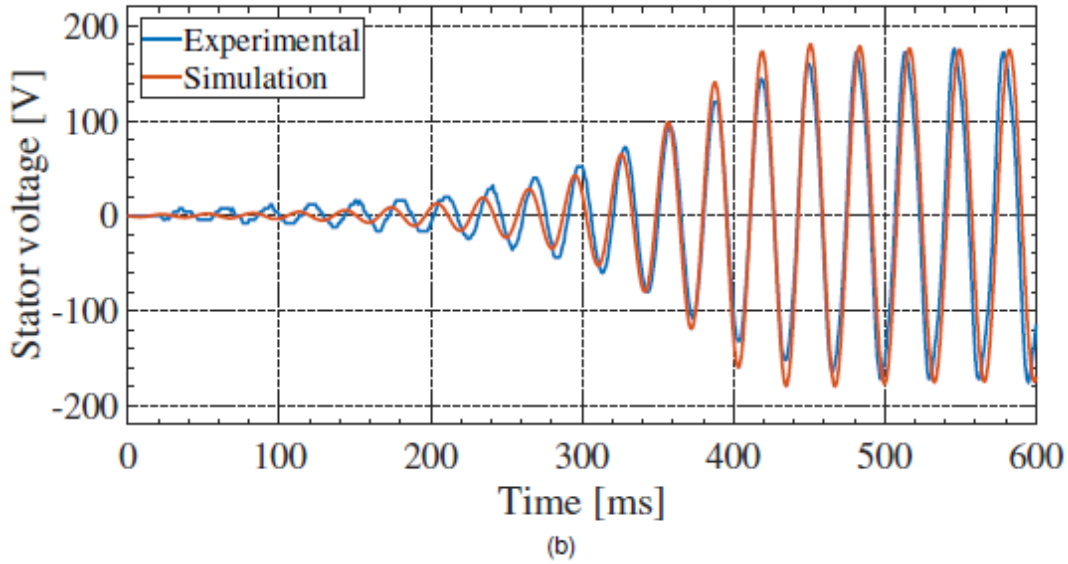

Figure 2.7: Terminal voltage of the SEIG while connecting the capacitor bank (switch on) for $R_L = 600\ \Omega$ and a phase capacitor of: (a) $C = 50$ µF; (b) $C = 70$ µF.

Table 2.2: Comparison of the steady state results between the experimental and simulated tests presented in Figure 2.7.

		Experimental	Model	Relative error
	N [rpm]	750	758	-1%
C = 50 µF	f_s [Hz]	35.2	35	0.7
	V_s [V]	144	145	-0.8%
	N [rpm]	660	666	-0.9%
C = 70 µF	f_s [Hz]	30.8	30.3	1.5%
	V_s [V]	125	123	1.7%

could produce. Note that a smaller resistive value means a higher consumed current by the load. Since the reactive power supplied by the capacitor and the mechanical power supplied by the DC motor did not increase, the generator could not meet the demand and the system stabilized with lower active power.

The results present in Table 2.3 show that, for the load of $R_L = 300\ \Omega$, final values of V_s and I_s obtained in the experimental tests are smaller than the ones obtained in the simulations, which resulted in lower active power supplied to the load. Besides this, it can also be seen in the experimental results that when the load increased slightly (the case of $R_L = 600\ \Omega$), the speed decreased, but when the load increased significantly (the case of $R_L = 300\ \Omega$) speed increased.

This being said, it appears that the behavior of the speed is different between the experiment and the simulation for $R_L = 300\ \Omega$. However, when analyzing the course of the speed in the simulation, speed was seen to increase to 852 rpm due to the decrease of active power produced by the SEIG, even though it did not reach its initial value of 856 rpm. This behavior shows a deviation from the minimum capacitance curves required to excite the machine as a speed function. For instance, for a load of $R_L = 250\ \Omega$ the speed obtained in simulations was already higher than its initial value.

Table 2.3: Comparison of the steady state results between the experimental and simulated tests presented in Figure 2.8.

		Experimental		Model		Relative error	
		Initial	Final	Initial	Final	Initial	Final
	[rpm]	839	834	847	834	-1.0	0.0
$R_L = 600\ [\Omega]$	f_s [Hz]	41.0	40.0	41.0	39.4	0.0 %	1.4 %
	V_s [V]	180	141	179	141	0.6 %	0.1 %
	I_s [A]	1.6	1.2	1.6	1.2	2.3 %	-2.3 %
	E/f [V Hz^{-1}]	4.4	3.5	4.4	3.6	0.6 %	-1.3 %
	N [rpm]	848	863	856	852	-1.0 %	1.2 %
$R_L = 300\ [\Omega]$	f_s [Hz]	41.2	40.3	41.3	39.2	-0.4 %	2.7 %
	V_s [V]	181	90	183	107	-1.4 %	-18.4 %
	I_s [A]	1.6	0.8	1.6	0.9	-1.0 %	-16.4 %
	E/f [V Hz^{-1}]	4.4	2.2	4.4	2.7	-1.1 %	-21.7 %

After validating the induction machine model, the PAT model was developed and tested as well. This

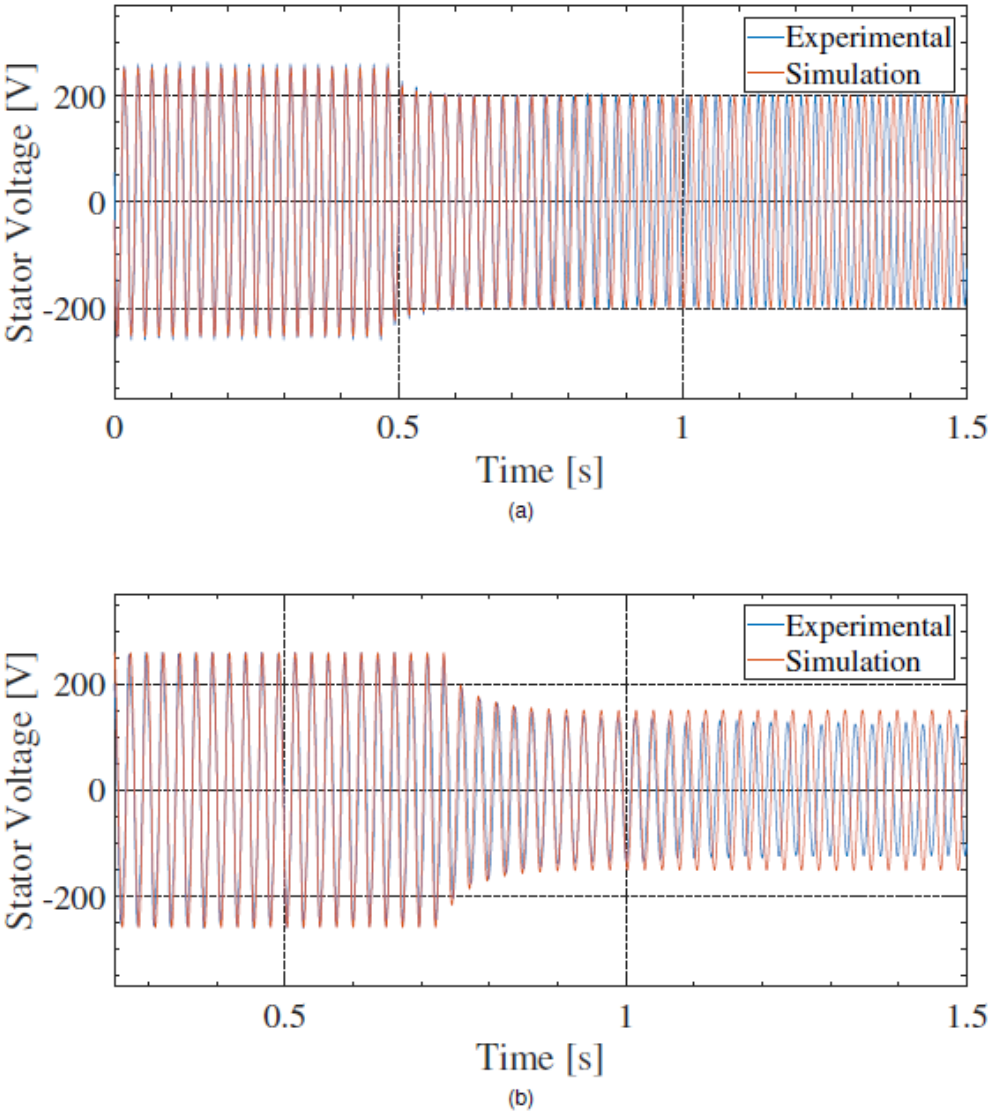

Figure 2.8: Terminal voltage of the SEIG while connecting the load and for $C = 35$ µF and a phase resistance of: (a) $R_L = 600\ \Omega$; (b) $R_L = 300\ \Omega$.

model is illustrated in Figure 2.9. The major conclusion from these tests was that hydraulic power and global efficiency increase with the pressure.

In the end, the behavior of groups of two PATs was evaluated. When the two generating units are connected in series, the two turbines' water flow rate must be the same, i.e., $Q_1 = Q_2$. Besides, the pressure drop associated with each of the PATs has to be equal to the total pressure imposed on the system: $P_{total} = P_1 + P_2$. Two major tests were performed to analyze the PATs group's behavior: decreasing and increasing either the load value or the capacitance value in one of the PAT and see how it affects the other PAT.

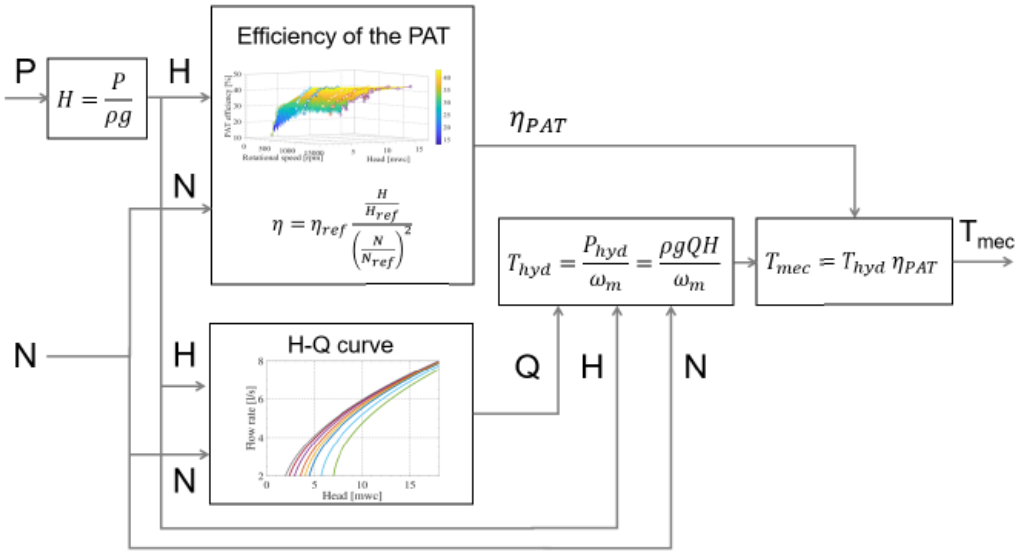

Figure 2.9: Complete model of the PAT developed in [9].

When decreasing either the load value of PAT2 R_{L2} or the capacitance value C_2, PAT2 speed N_2 increased and therefore flow rate Q_2 decreased. As the PATs are connected in series, Q_1 = Q_2, flow rate of PAT1 Q_1 will also decrease, and so will its head drop H_1. Since the total pressure P_{total} is constant, H_2 will be seen to increase. The increase of speed and head in PAT2 will result in the same hydraulic power transferred to PAT2 and the same power being consumed by its load. An increase of H_2 and a decrease of Q_2 will cancel out, and hydraulic power remains the same. Figure 2.10 shows speed, stator current, and stator active power for the group PAT2+SEIG2 for a decrease in the load R_{L2}.

Regarding the PAT1+SEIG1 group, the perturbation imposed on PAT2 will lower head, flow rate, and speed and consequently lower hydraulic power for PAT1, so its load will be consuming less active power. The opposite logic can be applied when the load value of PAT2 increases or the capacitance value C_2 increases. This brings upon an interesting conclusion: even though the load was changed in the second group, PAT2+SEIG2, the biggest impact is felt in the first group, PAT1+SEIG1.

Regarding the parallel connection, there is only one constraint in the parallel connection: P_1 and

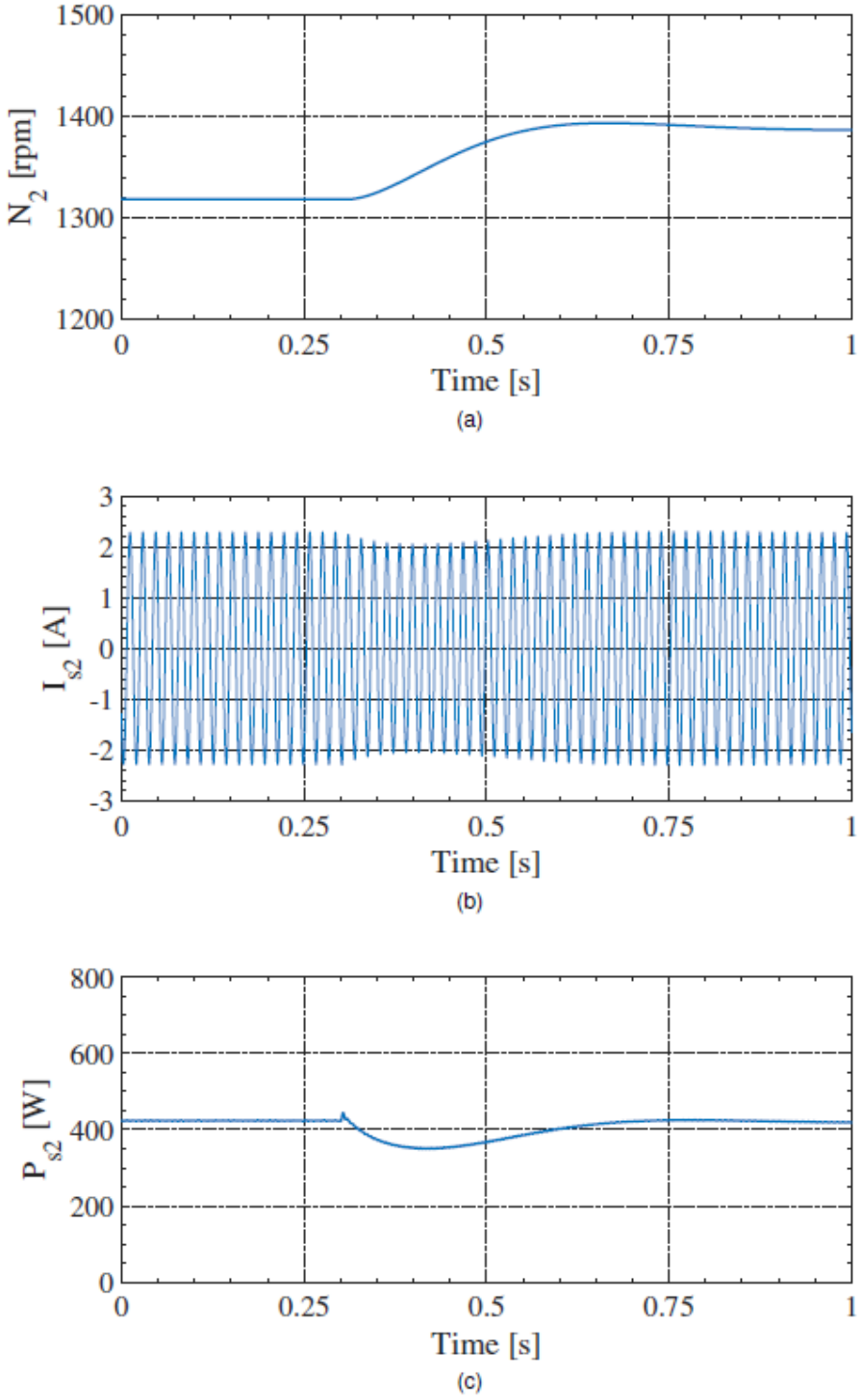

Figure 2.10: Test results when simulating a decrease of R_{L2} from $200\ \Omega$ to $160\ \Omega$, with Ptotal = 5×105 Pa and C_1 = C_2 = 23 µF.

P_2 must equal the pressure imposed to the complete generating system, P_{total}. Flow rates Q_1 and Q_2 change individually. This way, a change in one PAT's flow rate does not affect the other PAT, so the two subsystems are independent. A variation in the capacitance value C_2 or in the resistive load R_{L2} on the group PAT2+SEIG2 does not affect the other group, PAT1+SEIG1.

Following the previous works, in this thesis is intended to study the generating unit behaviour when speed, torque or mechanical power are being controlled and the generator is being fed by an inverter instead of being self-excited by a capacitor bank.

3

Field-Oriented Control algorithm

Contents

3.1 Introduction

Induction machines can be controlled in several ways. Usually, the most interesting control variables are speed, torque and flux. Scalar and vector controls are two different methods of controlling such variables.

Scalar control method is based on varying two quantities simultaneously: voltage and frequency. Speed can be controlled by varying frequency *f*, but this results in a change of impedances, which in turn results in a change of the current. Changing the current will change the torque produced by the machine. On the other hand, changing the voltage *E* can lead to saturation of the machine iron core. To avoid this problems, it is necessary to vary both voltage and frequency at the same time, so that the disadvantages of changing frequency and voltage can be compensated. Indeed, with a constant *E/f* ratio, a constant stator flux is maintained. Scalar control is a cheap method, but is not satisfactory for the control of drives with dynamic behaviour, since it provides slow transient responses.

The induction machine used in this thesis will be operating as a generator connected to a prime mover, in this case a pump operating as a turbine, which has a very dynamic behaviour. That being said, the main goal of this chapter is to develop a speed control scheme of an induction machine built around a field-oriented torque control system, which one of the vector control methods, and simulate it for the machine stand-alone operation, i.e, not connected to the PAT.

The first step is to develop the induction machine model. Differential equations characterize this model with time-varying inductances, which are dependent on the rotor position with respect to the stator reference axis. This leads to a complex set of equations to fully describe the induction machine in the usual stationary *abc* reference frame. To simplify the model, a rotating *dq0* reference frame will be adopted. To change from the *abc* frame to the *dq0* frame (*d*-direct, *q*-quadrature, *0* homopolar), the Park transformation is used. Considering a three-phase balanced system, the resultant homopolar quantities will be null, thus reducing the system from three (*dq0*) to two quantities (*dq*). Applying the Park transformation will then reduce three AC sinusoidal quantities in the *abc* frame into two DC quantities in the *dq* frame.

In this field-oriented control scheme it is possible to uncouple the field components: the direct-axis component of the stator current i_{ds} functions as the field current in a DC machine, setting the rotor direct-axis flux λ_{dr}, and torque is then determined by the quadrature-axis stator current i_{qs} just as the torque is determined by the armature current in a DC motor. The deduction of the induction machine model in the *dq* reference frame has been made previously in [9].

In the end, an inverter will be used to impose the three-phase voltages to the induction machine and the algorithm used to modulate that inverter.

3.2 Induction machine *dq* model

The reference frame used to deduce the induction machine equations is present in Figure 3.1.

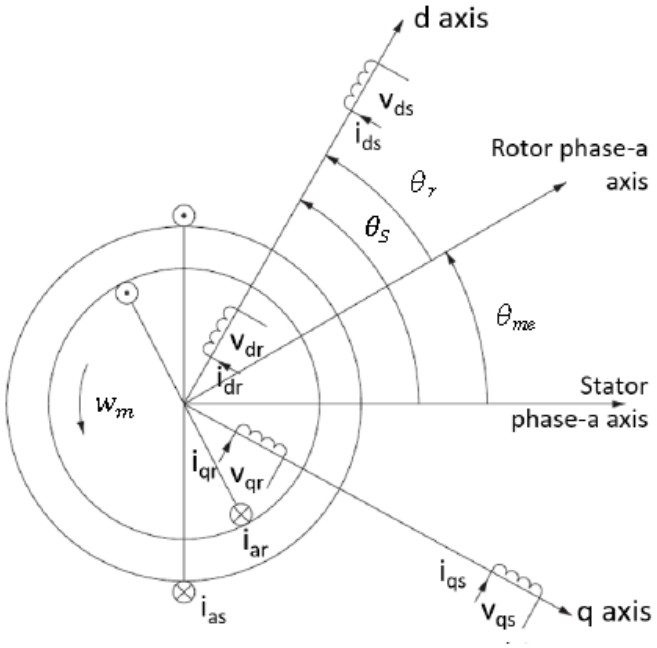

Figure 3.1: Synchronously rotating *dq* reference frame overlapped onto the three-phase reference frame of an induction machine.

From Figure 3.1 one can obtain the following equations

$$\theta_s = \theta_r + \theta_{me} \tag{3.1}$$

$$\theta_{me} = \theta_m \frac{poles}{2}, \tag{3.2}$$

where θ_s is the electrical angle between stator and *d* frame axis, θ_r is the electrical angle between rotor and *d* frame axis, θ_{me} is the electrical angle between stator and rotor, which is given by the mechanical angle θ_m multiplied by the number of pole pairs of the machine.

3.2.1 Voltages equations

Considering v_{ds}, v_{qs}, i_{ds}, i_{qs}, λ_{ds} and λ_{qs} are the *d* and *q* stator voltages, currents and linkage fluxes, v_{dr}, v_{qr}, i_{dr}, i_{qr}, λ_{dr} and λ_{qr} the rotor's voltages, currents and linkage fluxes and w_s and w_r the electrical frequency of the stator and rotor related to the *d*-axis. The Faraday's law applied to the induction machine in this reference frame results in

$$v_{ds} = R_s i_{ds} + \frac{d}{dt}\lambda_{ds} - w_s \lambda_{qs} \tag{3.3}$$

$$v_{qs} = R_s i_{qs} + \frac{d}{dt}\lambda_{qs} + w_s \lambda_{ds} \tag{3.4}$$

$$v_{dr} = R_r i_{dr} + \frac{d}{dt}\lambda_{dr} - w_r \lambda_{qr} = 0 \tag{3.5}$$

$$v_{qr} = R_r i_{qr} + \frac{d}{dt}\lambda_{qr} + w_r \lambda_{dr} = 0 \tag{3.6}$$

Rotor voltages in the *dq* reference frame v_{dr} and v_{qr} are null because the induction machine being used is of the squirrel-cage type.

3.2.2 Flux equations

The relation between the stator and rotor fluxes with the currents are described bellow:

$$\lambda_{ds} = L_s i_{ds} + L_m i_{dr} \tag{3.7}$$

$$\lambda_{qs} = L_s i_{qs} + L_m i_{qr} \tag{3.8}$$

$$\lambda_{dr} = L_r i_{dr} + L_m i_{ds} \tag{3.9}$$

$$\lambda_{qr} = L_r i_{qr} + L_m i_{qs} \tag{3.10}$$

The inductances L_s and L_r are given by

$$L_s = L_m + l_{\sigma s} \tag{3.11}$$

$$L_r = L_m + l_{\sigma r}, \tag{3.12}$$

where $l_{\sigma s}$ and $l_{\sigma r}$ represent the stator and rotor leakage inductances, respectively, and are assumed to be constant. As shown in [8], the magnetizing inductance of the machine L_m is the parameter that influences the induction machine dynamics the most. For the machine being used in this work (Table 2.1) it was verified that L_m changes according to the following equation

$$L_m = 0.0025\left(\frac{E}{f}\right)^3 - 0.041\left(\frac{E}{f}\right)^2 + 0.12\left(\frac{E}{f}\right) + 0.53 \text{ [H]}, \tag{3.13}$$

where *E* represents the magnetization voltage and *f* the electrical frequency. Assuming sinusoidal quantities, the magnetization level *E/f* is approximately given by

$$\frac{E}{f} \approx \frac{2\pi\lambda_M}{\sqrt{2}} \tag{3.14}$$

and the mutual flux λ_M given by

$$\lambda_M = \sqrt{(\lambda_{ds} - L_s i_{ds})^2 + (\lambda_{qs} - L_s i_{qs})^2}. \tag{3.15}$$

3.2.3 Active power, reactive power and mechanical coupling equations

The stator active power is given by

$$P_s = \frac{3}{2}(v_{ds} i_{ds} + v_{qs} i_{qs}) \tag{3.16}$$

and the stator reactive power is given by

$$Q_s = \frac{3}{2}(v_{qs} i_{ds} - v_{ds} i_{qs}) \tag{3.17}$$

To finalize the model, one needs to have an equation that relates the torque produced by the induction motor T_e with its shaft speed of rotation w_m. This mechanical coupling equation is given by

$$J\frac{dw_m}{dt} = T_e - T_L - T_{losses}, \tag{3.18}$$

where *J* represents the moment of inertia of the shaft, T_L the external load torque applied to the shaft and T_{losses} the friction inherent to the shaft rotation. For this application, the losses torque was measured experimentally, being proportional to the speed of the induction machine, defined as

$$T_{losses} = 0.001 w_m \text{ [N m]} \tag{3.19}$$

3.3 Ideal case of operation

In this section, the field-oriented control algorithm for speed control of the induction machine is developed. The initial approach is the ideal case of operation, where the voltages to be applied to the machine are the output of PI controllers. Figure 3.2 contains a schematic of the complete FOC control algorithm.

3.3.1 Field-Oriented Control algorithm

The field-oriented control algorithm applied to the induction machine allows control of its speed of rotation. The algorithm must be able to, given an input reference speed, estimate the rotating magnetic field and produce the reference voltages that will be applied to the machine's stator to achieve the desired speed.

Aligning the direct axis of the reference frame with the rotor flux gives

$$\lambda_{qr} = 0. \tag{3.20}$$

In steady-state, where the derivatives are null, solving Eq.(3.6) one gets

$$w_r = -R_r \frac{i_{qr}}{\lambda_{dr}} \tag{3.21}$$

Solving Eq.(3.10) for i_{qr} gives

$$i_{qr} = -\frac{L_m}{L_r} i_{qs}. \tag{3.22}$$

Substituting this result in Eq.(3.21) and applying it to Eq.(3.1) gives

$$w_s = w_{me} + \frac{R_r}{L_r} \frac{i_{qs}}{i_{ds}}. \tag{3.23}$$

Integrating w_s one obtains the estimation of the electrical position of the rotating magnetic field concerning the stator geometry position, that is θ_s, that will be used to convert the *dq* quantities into the three phase *abc* quantities

$$\theta_s = \int w_s \, dt = \int \left(w_{me} + \frac{R_r}{L_r} \frac{i^*_{qs}}{i^*_{ds}} \right) dt. \tag{3.24}$$

The measured currents i_{ds} and i_{qs} were replaced by their reference values i^*_{ds} and i^*_{qs} because the currents will be controlled by PI (proportional-integral) controllers, so they are the same in steady-state. Maintaining $\lambda_{qr} = 0$, solving Eq. (3.5) for i_{dr} gives in steady-state

$$i_{dr} = 0, \tag{3.25}$$

which, substituting in Eq.(3.9) gives

$$i^*_{ds} = \frac{\lambda^*_{dr}}{L_m}. \tag{3.26}$$

This quantity represents the reference stator current in the direct axis. The reference rotor flux λ^*_{dr},

which is the total rotor flux, can be chosen arbitrarily. Knowing the machine nominal single-phase voltage V_n and nominal frequency f_n, one can start by using the nominal flux given by

$$\lambda_{dr}^{*} \approx \frac{\sqrt{2}V_n}{2\pi f_n}. \tag{3.27}$$

To calculate the reference quadrature current, one will use the electromagnetic torque formula

$$T_e = \frac{3}{2}\frac{p}{2}\frac{L_m}{L_r}\lambda_{dr} i_{qs}, \tag{3.28}$$

that can be written as

$$i_{qs}^{*} = \frac{2}{3}\frac{2}{p}\frac{L_r}{L_m}\frac{T_e^{*}}{\lambda_{dr}^{*}}. \tag{3.29}$$

The only variable missing to calculate this current is the reference motor torque T_e^{*}. In the first approach, the algorithm will be controlling speed. Therefore, T_e^{*} will be defined as the output of a PI controller, whose input will be the difference between the reference motor speed $w_{m_{ref}}$ and the actual speed of rotation w_m.

To complete the algorithm, stator voltages in the *dq* reference frame will be defined as the outputs of PI controllers that control the machine stator currents. Their input will be the difference between the reference currents i_{ds}^{*} and i_{qs}^{*} and i_{ds} and i_{qs} that are obtained from the measured currents. Using the estimated angle θ_s obtained in (3.24), one can compute the three-phase voltages in the *abc* reference frame that will be applied to the induction machine through the power-invariant inverse Park transformation.

3.3.2 Numerical results of the FOC algorithm

In this section the numerical results obtained in the computational simulations are presented. The software used for performing the tests was MATLAB®/ Simulink. The nominal data of the induction machine used to test the algorithm is presented in Table 2.1. The algorithm will be tested for the machine running at no load (no external torque T_L applied).

The first step is to tune the PI controllers' proportional gains P and integral gains I, whose transfer function is given by

$$C(s) = P + \frac{I}{s} \tag{3.30}$$

To do that, the reference speed was assumed to be a step waveform with magnitude equal to the nominal speed (910 rpm) and the rotor flux equal to the rated flux

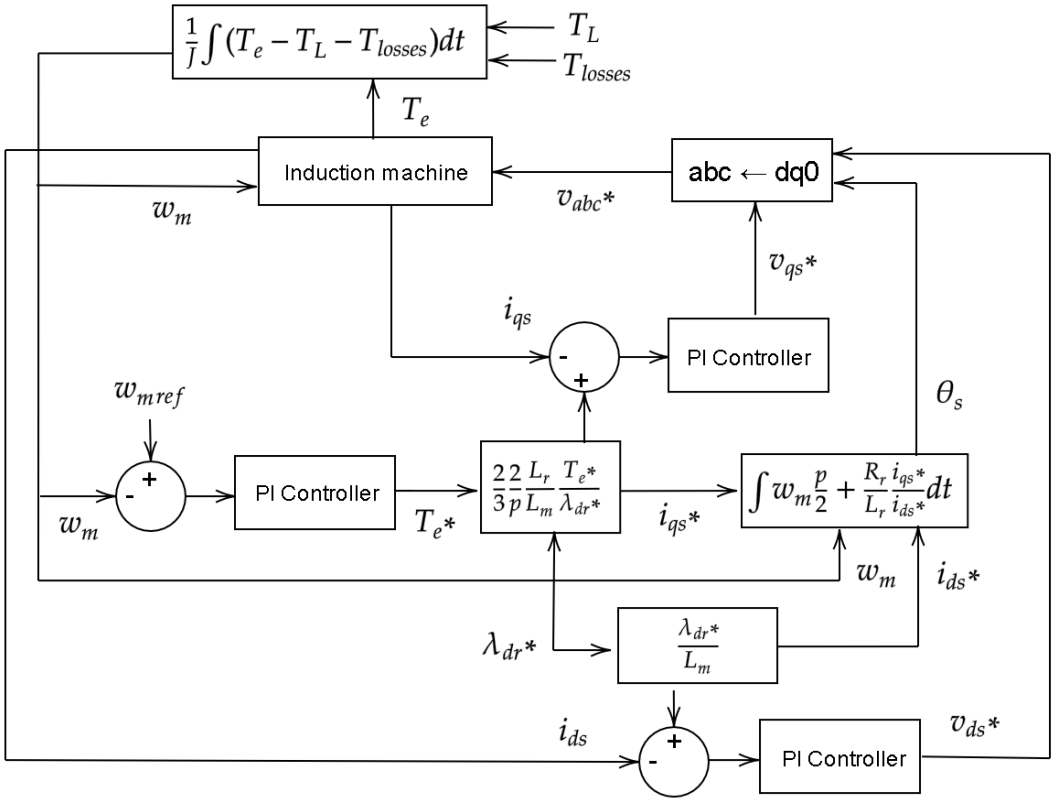

Figure 3.2: Ideal case of operation: Field-Oriented control algorithm for speed control.

$$\lambda_{dr}^{*} \approx \frac{400\sqrt{2/3}}{2\pi \times 50} \approx 1,04 \text{ Wb.} \tag{3.31}$$

For this specific machine, a satisfactory convergence time is in the order of tenth of a second at no load, since it has a very small inertia.

Tuning the gains was made by trial-error process. One can start by setting all proportional gains equal to 1 and integral gains equal to 100. It can be seen (Figure 3.3) that the machine speed converges at a very slow pace, as it takes more than 1 second to achieve the desired speed, which means that the proportional gains are still too low. There are also oscillations in the convergence region, meaning that the integral gains are also small.

Increasing the gains to P = 10 and I = 1000 led to the results present in Figure 3.4. As shown, the speed of convergence is now satisfactory (0.4 s), but the motor speed still oscillates around the reference value. This means that the PI controller responsible for the reference torque T_e^* is now tuned, but the PI controllers that control currents and set the voltages are not. That being said, looking at the currents in the *dq* reference frame is a good way to know if the current controllers are behaving correctly (Figure 3.5).

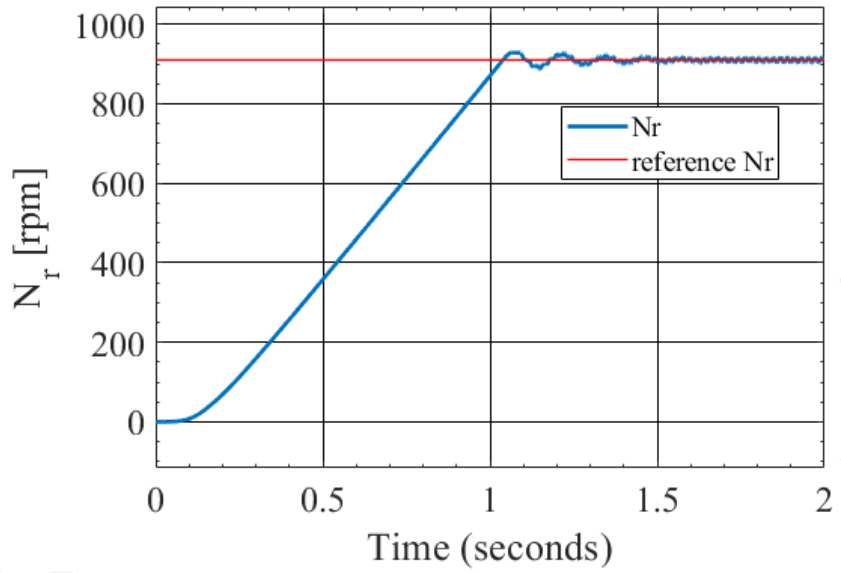

Figure 3.3: Ideal case of speed control: speed for P = 1, I = 100.

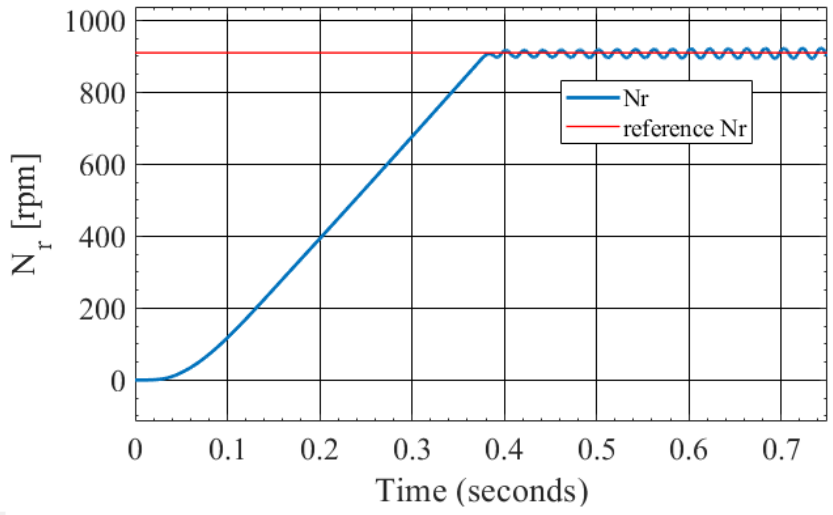

Figure 3.4: Ideal case of speed control: speed for P = 10, I = 1000.

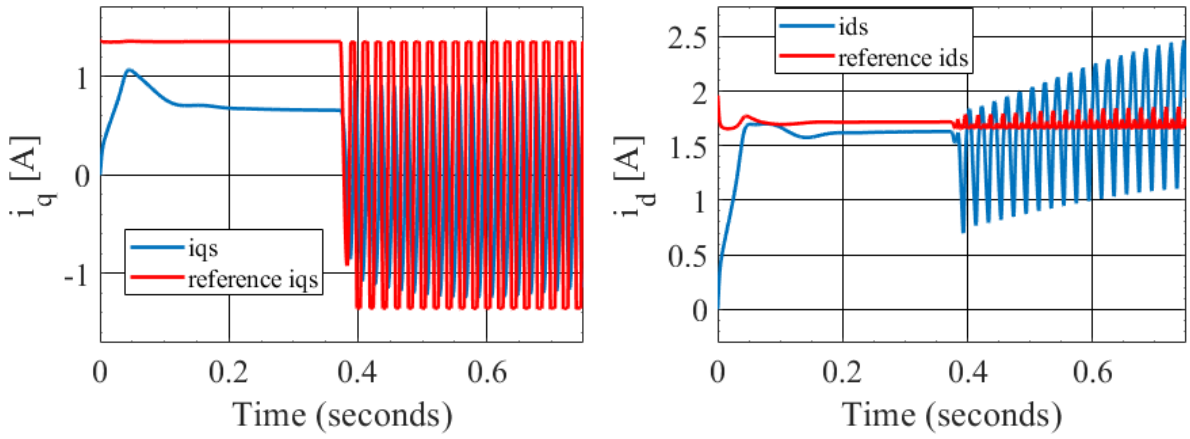

Figure 3.5: Ideal case of speed control: i_{qs} (left) and i_{ds} (right) current for P = 10, I = 1000.

Observing Figure 3.5, one concludes that the currents are not following the reference ones. To tune the two PI controllers that produce the reference stator voltages, it will be set P = 1000 and I = 10000, leaving the proportional and integral gains of the torque controller untouched (P = 10, I = 1000). The final results are satisfactory (Figures 3.6, 3.7 and 3.8). Indeed, the convergence speed was maintained, as the torque controller was already tuned, but the oscillations were removed and the currents are now following the reference ones (Figure 3.7). There is a sudden change in the magnetizing current i_{ds} when convergence is achieved that can be explained by the evolution of the magnetizing inductance present in Figure 3.8. As shown, L_m is at its maximum value, which will result in a lower i_{ds} current.

Figure 3.9 illustrates the evolution of the stator current and voltage at the motor terminals. It can be seen that, while the reference speed is not achieved, current has a higher peak value and voltage a lower peak value. As speed increases, current peak drops and voltage stabilizes. This concludes the PI controllers tuning.

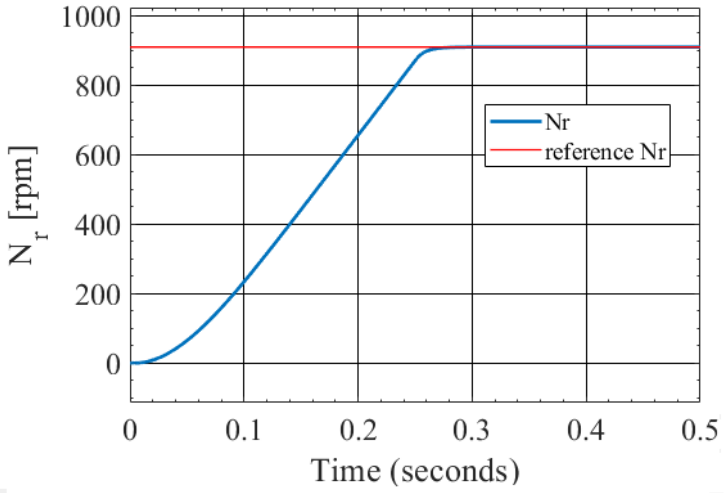

Figure 3.6: Ideal case of speed control: motor speed for P = 10, I = 1000 (torque controller), P = 1000, I = 10000 (current controllers).

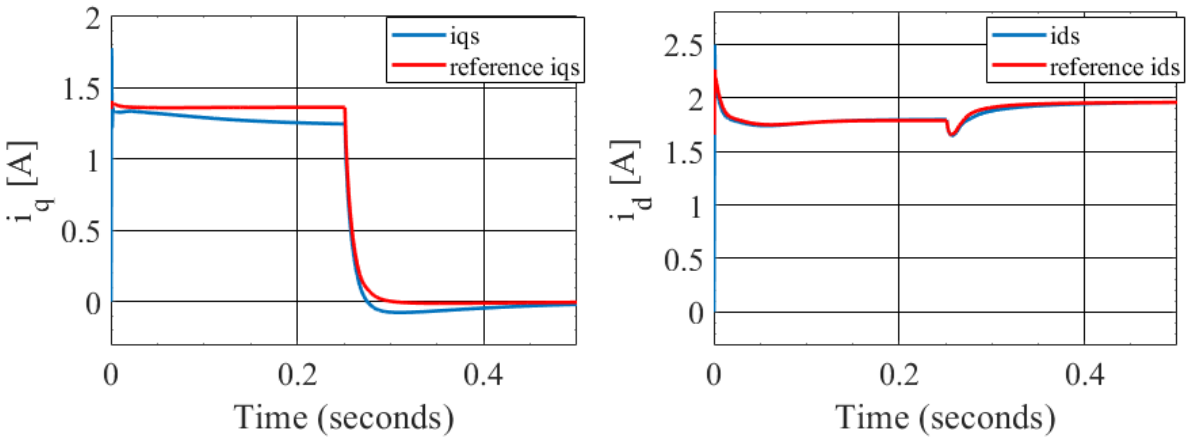

Figure 3.7: Ideal case of speed control: i_{qs} (left) and i_{ds} (right) currents for P = 10, I = 1000 (torque controller), P = 1000, I = 10000 (current controllers).

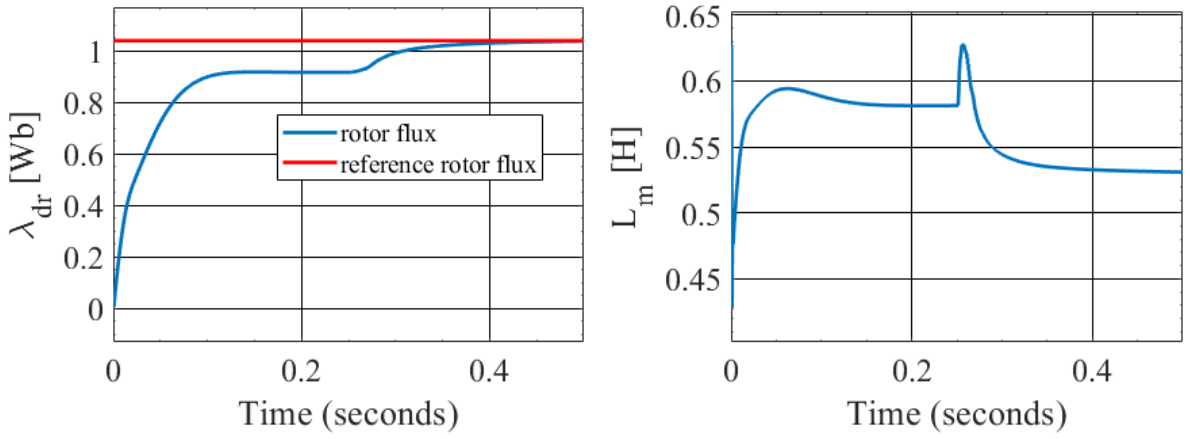

Figure 3.8: Ideal case of speed control: rotor flux (left) and magnetizing inductance (right) for P = 10, I = 1000 (torque controller), P = 1000, I = 10000 (current controllers).

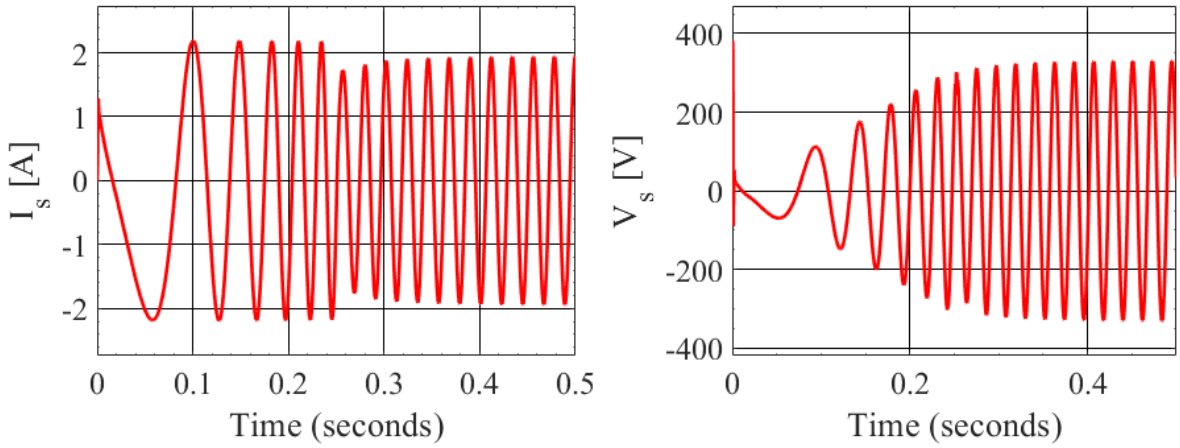

Figure 3.9: Ideal case of speed control: stator current (left) and single-phase voltage (right) for P = 10, I = 1000 (torque controller), P = 1000, I = 10000 (current controllers).

3.4 Inverter-case

In this section, it is analysed the inclusion of a voltage converter to drive the induction machine. Previously, the reference voltages were generated by two PI controllers, converted from the *dq* reference frame to three *abc* voltages and applied directly to the machine (see Figure 3.2). This case is ideal since the controllers can provide perfectly sinusoidal voltages, although they have been limited to the machine's nominal voltage. Thus, it is now of major interest to test how the results are affected if the voltages are produced by a three-phase inverter fed by a battery, i.e., including the harmonic content generated by the inverter. In generator mode, the battery that feeds the inverter is the induction machine load.

The reference voltages v_{ds}^* and v_{qs}^* will now be used to generate the gate signals that drive the inverter switches through the SVPWM modulation method (*Space Vector Pulse Width Modulation*). The two quantities that characterize voltage and are used to generate the gate signals are magnitude and angle. To obtain them, the first step is to convert these voltages into the $\alpha - \beta$ reference frame. The power invariant transformation from the *abc* reference frame to the $\alpha - \beta$ reference frame is given by

$$\begin{bmatrix} v_\alpha \\ v_\beta \end{bmatrix} = \sqrt{\frac{2}{3}} \begin{bmatrix} 1 & -\frac{1}{2} & -\frac{1}{2} \\ 0 & \frac{\sqrt{3}}{2} & -\frac{\sqrt{3}}{2} \end{bmatrix} \begin{bmatrix} v_a \\ v_b \\ v_c \end{bmatrix} \tag{3.32}$$

Magnitude of the reference voltage is given by

$$V_{abc_{peak}} = \sqrt{v_\alpha^2 + v_\beta^2} \tag{3.33}$$

and the voltage angle can be calculated as

$$\alpha = \arctan\left(\frac{v_\beta}{v_\alpha}\right) \tag{3.34}$$

With SVPWM method [10], the magnitude of the fundamental component of the inverter output voltage is given by

$$V_{0_{peak}} = \frac{2V_{DC}}{\pi} \tag{3.35}$$

In the linear region, the modulation index can be expressed as

$$m = \frac{V_{abc_{peak}}}{V_{0_{peak}}} = \frac{\pi\sqrt{v_\alpha^2 + v_\beta^2}}{2V_{DC}} \tag{3.36}$$

The complete scheme illustrating the inverter inclusion is present in Figure 3.10. The inverter used in simulations was a IGBT three-leg inverter, fed by a DC voltage source of $V_{DC} = 600$ V. The inverter data is present in Table 3.1. The switching frequency used in the generation of the gate signals was f_s = 1.5 kHz.

Table 3.1: Nominal data of the IGBT inverter used to fed the machine.

Snubber resistance	10 kΩ
Snubber capacitance	∞
Internal resistance	1 mΩ
IGBT forward voltage	1.2 V
Diode forward voltage	1.2 V
DC link capacitance	2 mF

Evolution of the machine speed is shown in Figure 3.11. Comparing the results with the ones present in Figure 3.6 it can be concluded that using the inverter to feed the machine does not affect speed.

Figure 3.13 shows the evolution of rotor flux λ_{dr} and magnetizing inductance L_m. Comparing the results with the previous ones (Figure 3.8), the flux rises faster to the reference value when the inverter is driving the machine. This is because of the harmonic content of the voltage (Figure 3.12), increasing its total RMS value, which increases the magnetizing flux of the machine. The harmonics' effect in the voltage is also seen in the magnetizing inductance shape, with oscillations in the convergence region. Current is not distorted because the machine behaves like a passive RL filter.

Figure 3.14 shows the evolution of the stator currents i_{ds} and i_{qs}. Comparing the results obtained with the ones present in Figure 3.7, one concludes that they are similar to whether the motor is fed by the ideal voltages or by the inverter, which validates the inverter model and the modulation method used.

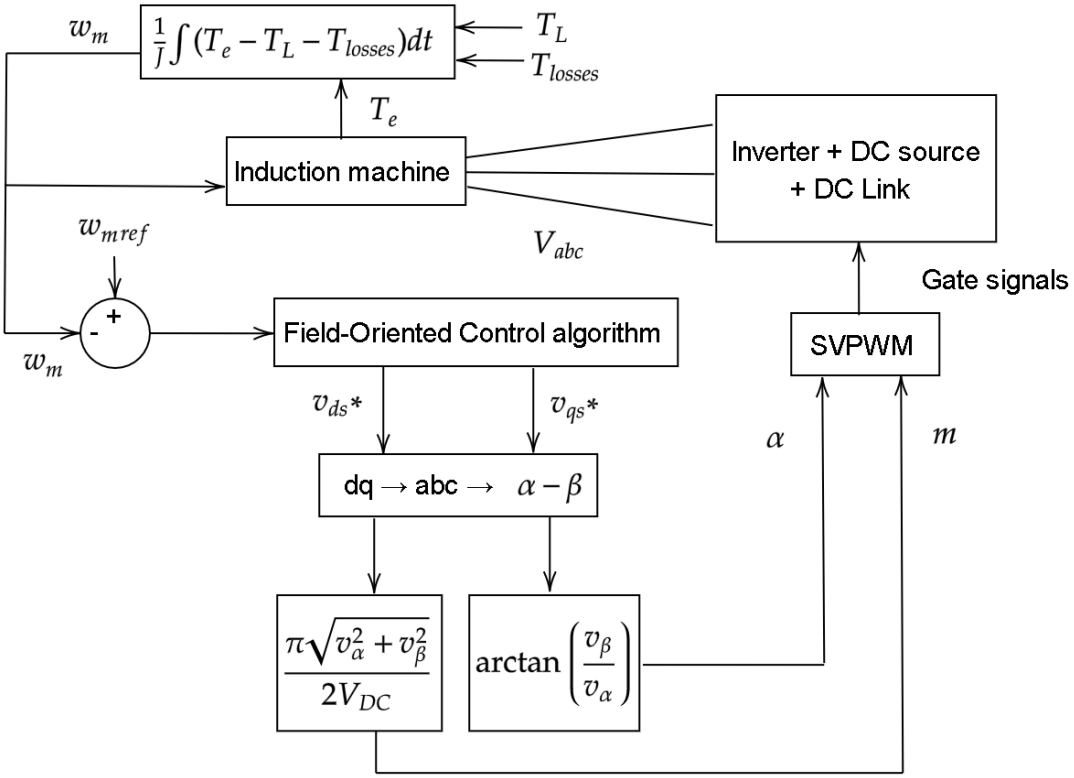

Figure 3.10: Field-Oriented control scheme for speed control with inverter.

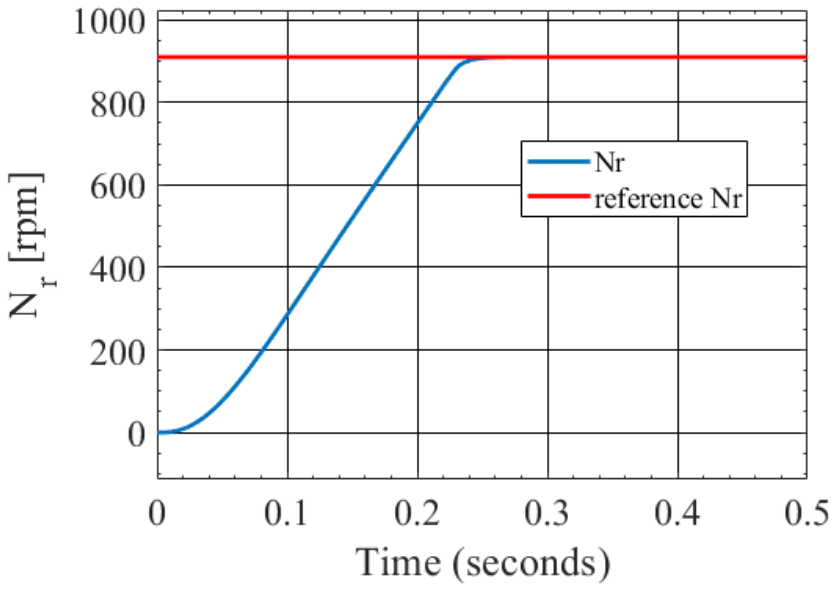

Figure 3.11: Inverter-based case speed control: machine speed for operation at no load (no external torque T_L applied).

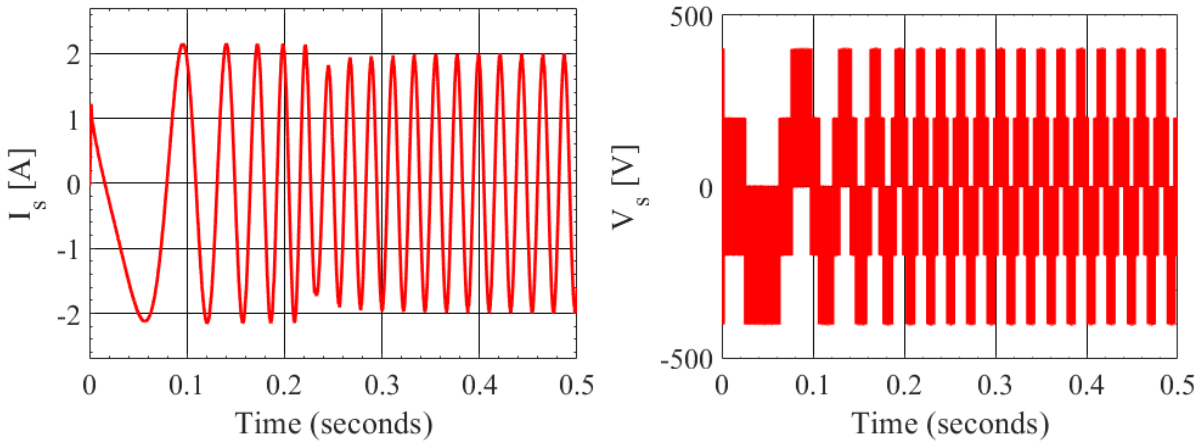

Figure 3.12: Inverter-based case speed control: stator current (left) and single-phase stator voltage (right).

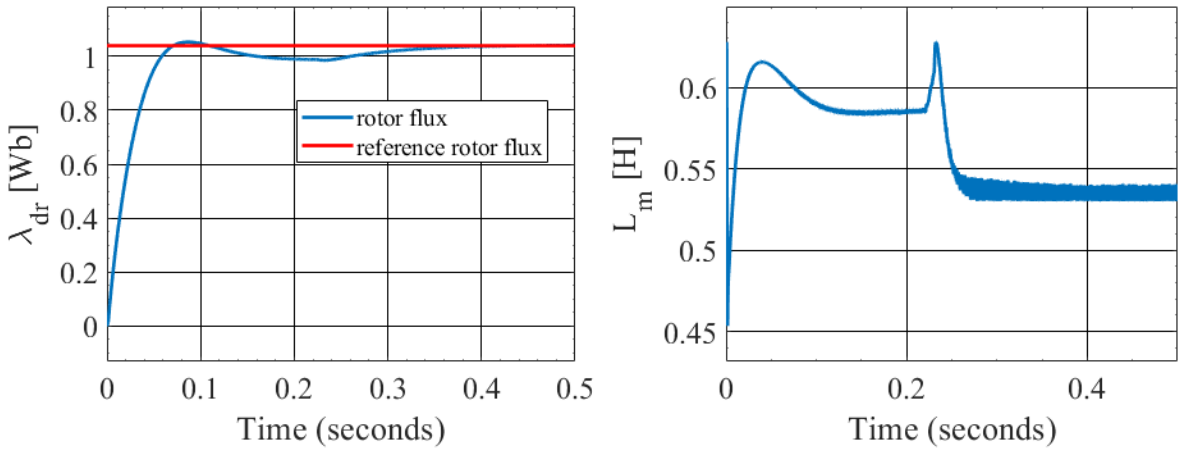

Figure 3.13: Inverter-based case speed control: λ_{dr} (left) and L_m (right) for P = 10, I = 1000 (torque controller), P = 1000, I = 10000 (current controllers).

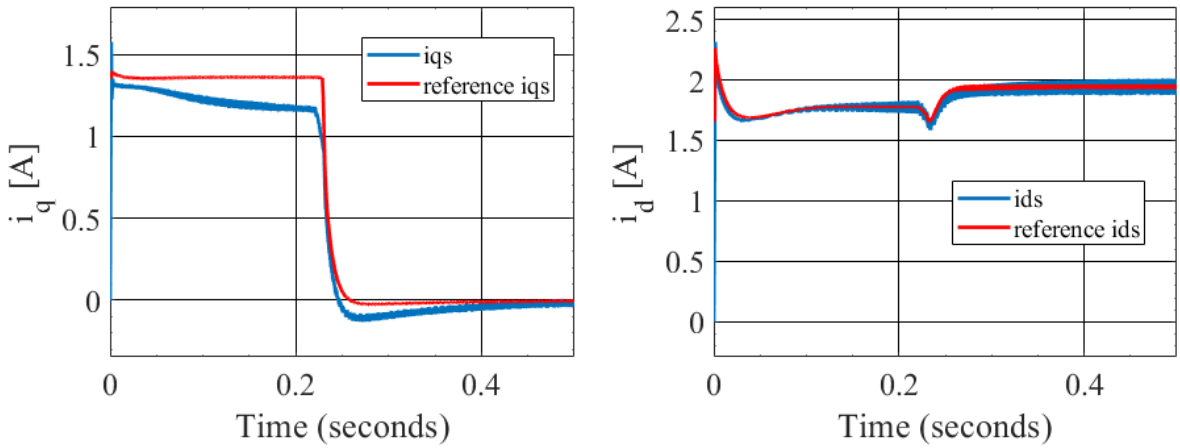

Figure 3.14: Inverter-based case speed control: i_{qs} (left) and i_{ds} (right) current for P = 10, I = 1000 (torque controller), P = 1000, I = 10000 (current controllers).

4

Electromagnetic torque and mechanical power control

Contents

4.1 Introduction

So far, the case that has been studied is the one in which the speed of rotation of the machine is controlled. Once this study's major interest is to use the induction machine in a generating unit, it is now intended to study what other quantities can be controlled. This chapter will address two ways of controlling the induction generator: electromagnetic torque control and mechanical power control. These quantities are related as follows

$$P_{mec} = T_e w_m \tag{4.1}$$

To perform the numerical study, it will be assumed that the machine is running at a constant speed equal to its nominal one (910 rpm) and rotor flux is equal to the rated flux ($1,04$ Wb). Since speed is assumed to be constant, torque or mechanical power control are equivalent, i.e., one can know torque when imposing a mechanical power reference value and vice-versa. In chapter 5, the PAT is included in the model and control of torque and mechanical power will no longer be equivalent because speed is not known beforehand.

Initially, this study will be carried out based on the ideal case of operation, where the voltages to be applied to the machine are the output of the current PI controllers without any electronic power converter. When powered by the controlled inverter, the induction machine's behavior will be analyzed, as done in the previous chapter.

4.2 Ideal case of operation

As shown in Figure 3.2, the reference torque used to calculate the reference current i_{qs}^* was obtained from the rotor and reference speeds. When performing torque control, the reference torque value will now be constant and enforced. Note that the imposed values will be negative, meaning that the machine will be operating in generator mode, as intended. According to the data present in Table 2.1, the nominal machine torque can be calculated as

$$T_e = \frac{P_n}{w_n} = \frac{550}{910 \times \frac{2\pi}{60}} \approx 5,8 \text{ N m} \tag{4.2}$$

In this situation, the torque PI torque will not be used since the torque value is the reference signal. Thus, the only PI controllers that will be tested are the currents i_{qs} and i_{ds} controllers.

The complete scheme used for electromagnetic torque control is shown in Figure 4.1.

To control the mechanical power on the machine shaft, the torque PI controller's input, whose output will be the reference torque, will be the difference between the reference power and the power on the

shaft. If the power at a given moment is less than the reference power, the difference will be positive, which will increase torque. As the speed of rotation is constant, this translates into an increase of mechanical power, as can be concluded through Eq.(4.1). The complete scheme used for mechanical power control is present in Figure 4.2.

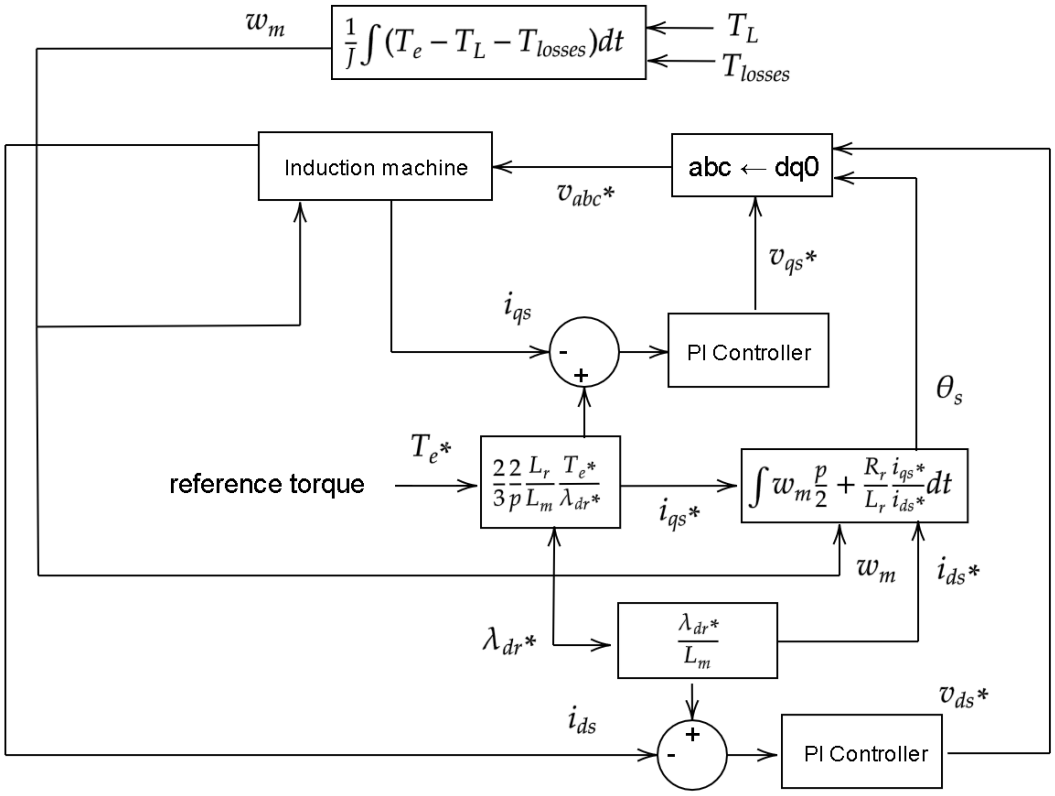

Figure 4.1: Field-Oriented control scheme for the ideal case of torque control.

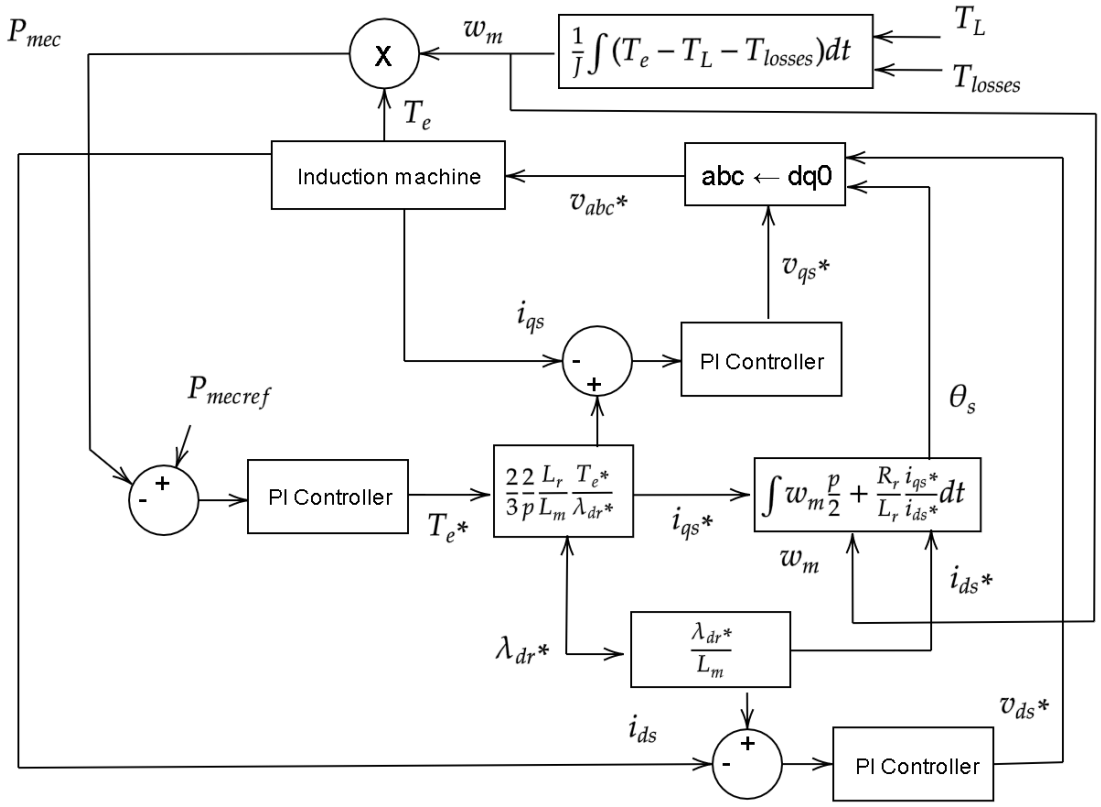

Figure 4.2: Field-Oriented control scheme for the ideal case of mechanical power control.

4.2.1 Electromagnetic torque control

The final gains obtained for electromagnetic torque control are P = 100 and I = 100000. A first test was performed for the nominal torque ($5,8$ N m) and the results are shown in Figure 4.3. By observing Figure 4.3 it can be seen that the desired torque is achieved within 0.2 s, which is a satisfactory convergence time for this machine as seen previously in speed control.

Figure 4.4 shows the currents evolution. As shown, the reference currents are followed, although there is a peak in i_{qs} current. Since one is imposing torque, which is commanded by i_{qs}, a sudden change in its value will result in abrupt changes in this current, although it has been limited to the rated current.

Figure 4.5 depicts single-phase stator voltage and current. Comparing the results with the ones present in Figure 3.9, it is shown that steady-state regime of voltage and current is achieved faster than in speed control. This happens because speed is imposed at start when performing torque control. Finally, as a way of systematizing the results, the generator efficiency, stator active power and reactive power were computed for different values of the reference electromagnetic torque. The results are present in Figures 4.6 and 4.7. For this tests, the nominal rotor flux was used as the reference flux to calculate the reference i^*_{ds} current. The maximum generator efficiency obtained was $60,2$ % for an electromagnetic torque of $-4,51$ N m. The efficiency of the machine in generator mode is given by

$$\eta_{gen} = \frac{P_s}{P_{mec}} \tag{4.3}$$

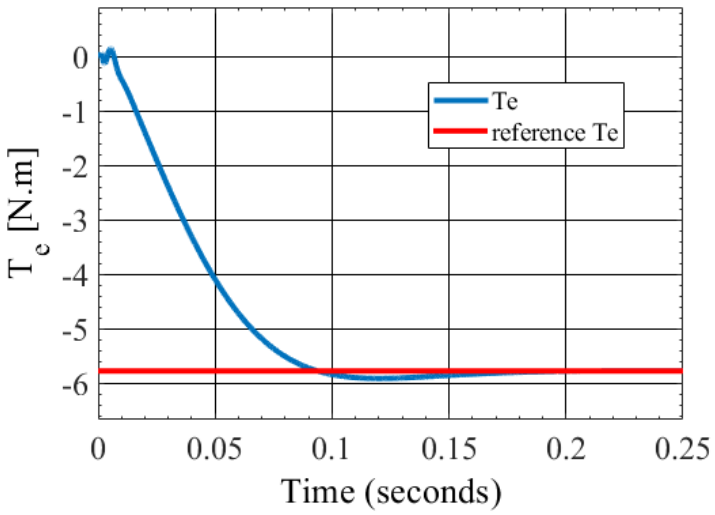

Figure 4.3: Ideal torque control: torque for P = 100, I = 100000 (current controllers).

.

Figure 4.7 shows that, for very low values of torque, the machine is operating in motor mode (con-

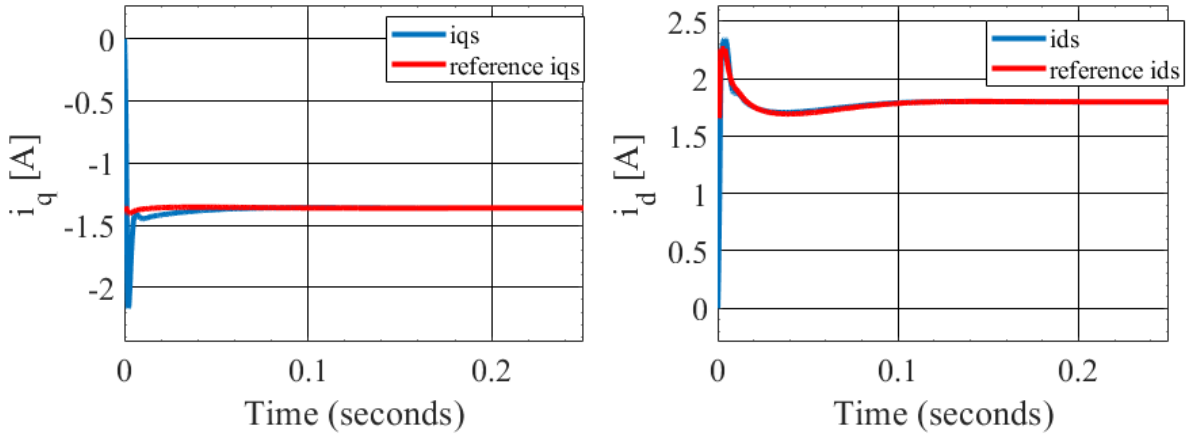

Figure 4.4: Ideal torque control: i_{qs} (left) and i_{ds} (right) currents for P = 100, I = 100000 (current controllers) for operation at rated torque.

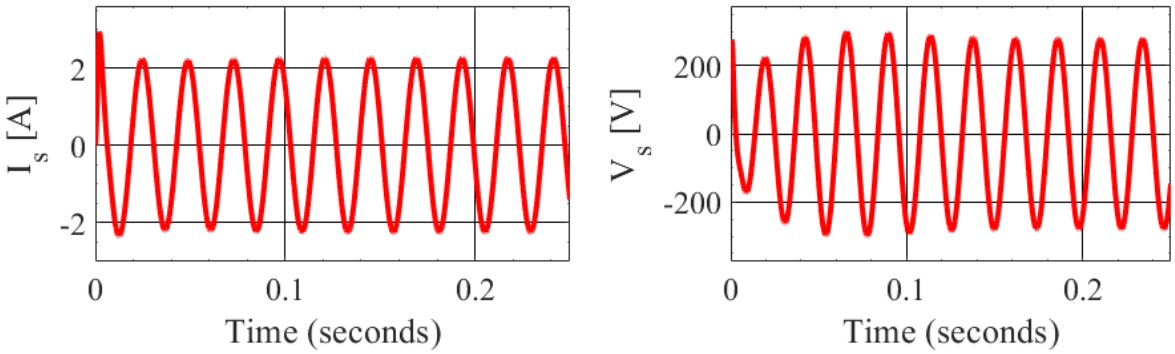

Figure 4.5: Ideal torque control: stator current (left) and single-phase voltage (right) for operation at rated torque.

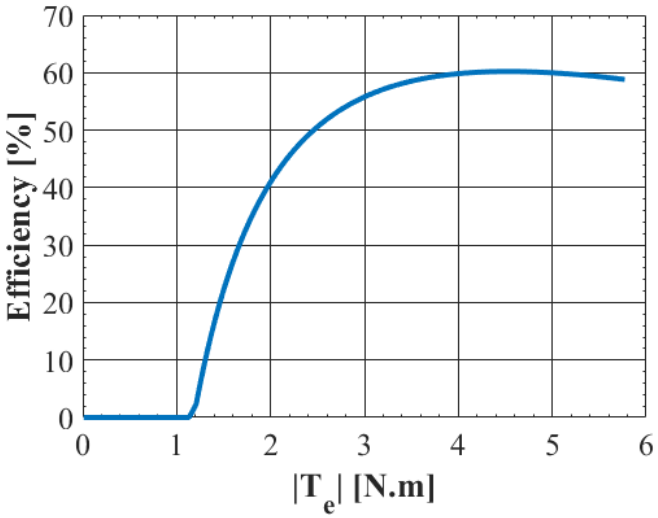

Figure 4.6: Ideal torque control: generator efficiency as function of the absolute value of electromagnetic torque.

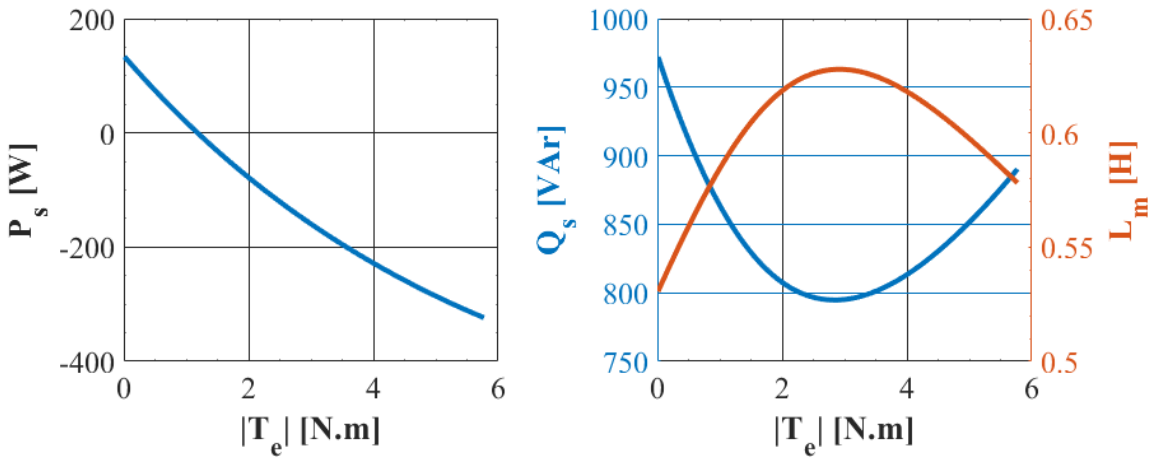

Figure 4.7: Ideal torque control: stator active power (left) and reactive power / magnetizing inductance (right) as function of the absolute value of electromagnetic torque.

suming active power) because stator active power is positive. In motor mode efficiency is not defined as in Eq.(4.3) and is instead given by P_{mec}/P_s. That is the reason why efficiency is shown to be zero for very low torques in Figure 4.6. There are two reasons why the machine may be operating in the motor mode for these values: the fact that the stator resistance is very high, which will result in high dissipated power due to the magnetization current, and the fact that the rotor flux is kept constant and equal to its nominal value for the entire range of operation. Low torques mean that the machine is operating in a partial load regime. Therefore, using rated flux to generate the magnetizing current i_{ds} will cause the machine's efficiency not to be the best possible.

Regarding reactive power, as shown in Figure 4.7, it is positive whether the machine is operating in motor mode or generator mode. This is because the induction machine needs to be magnetized regardless of its operating point, resulting in reactive power consumption.

There is a point of operation where consumed reactive power is minimum. This has to do with the magnetizing inductance value. Once rotor flux λ_{dr} is kept constant and equal to the rated value, the field-generating current i_{ds} will be smaller when L_m is higher, which in turn will result in lower reactive power consumed.

4.2.2 Mechanical power control

As done for torque control, a first test will be done for the nominal mechanical power of the machine (550 W). The torque controller values obtained in speed control (P = 10, I = 1000) will be maintained and the new values for the current controllers (P = 1000, I = 100000), obtained for the ideal torque control scenario in the previous section, will be used. Figure 4.8 shows the evolution of mechanical power and Figure 4.9 show i_{ds} and i_{qs} currents.

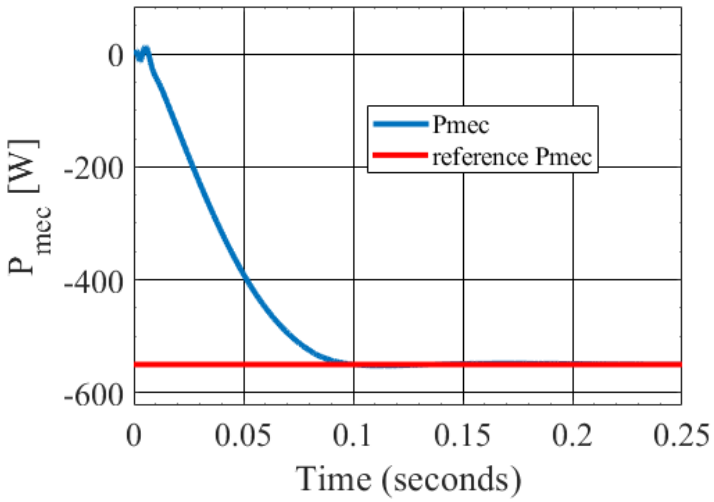

Figure 4.8: Ideal mechanical power control: mechanical power for P = 10, I = 1000 (torque controller) and P = 100, I = 100000 (current controllers) for operation at rated power.

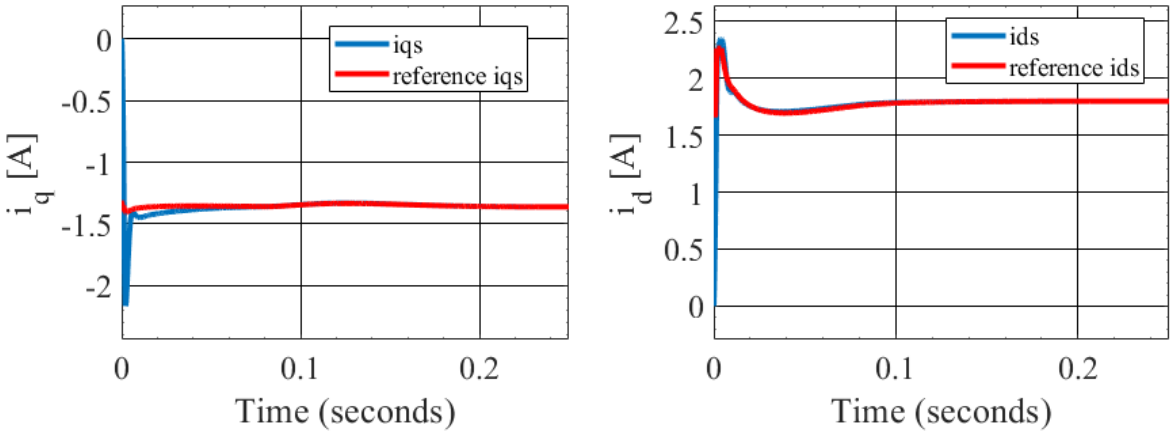

Figure 4.9: Ideal mechanical power control: i_{qs} (left) and i_{ds} (right) currents for P = 10, I = 1000 (torque controller) and P = 100, I = 100000 (current controllers) for operation at rated power.

As stated previously, since speed of rotation is kept constant, the torque and mechanical power control results must be equivalent. Comparing the results obtained for efficiency (Figure 4.10), active and reactive power (Figure 4.11) with the ones obtained for electromagnetic torque control it is concluded that this is in fact true. Maximum efficiency obtained was $60\ \%$ for a mechanical power of -429 W or a torque of $-4,5$ N m.

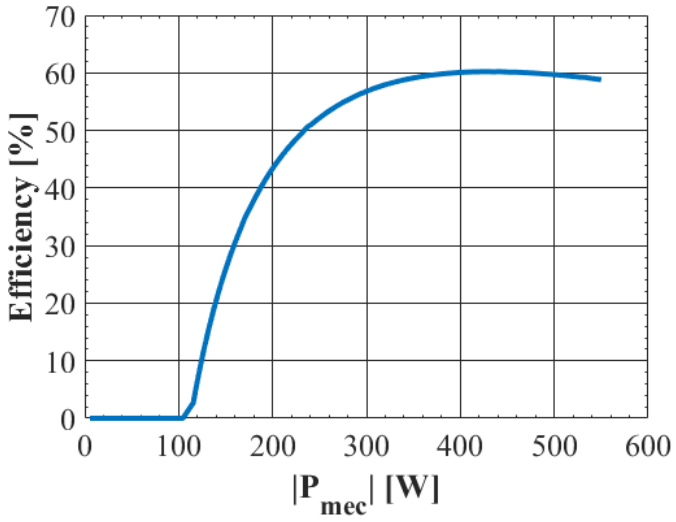

Figure 4.10: Ideal mechanical power control: generator efficiency as function of the absolute value of mechanical power.

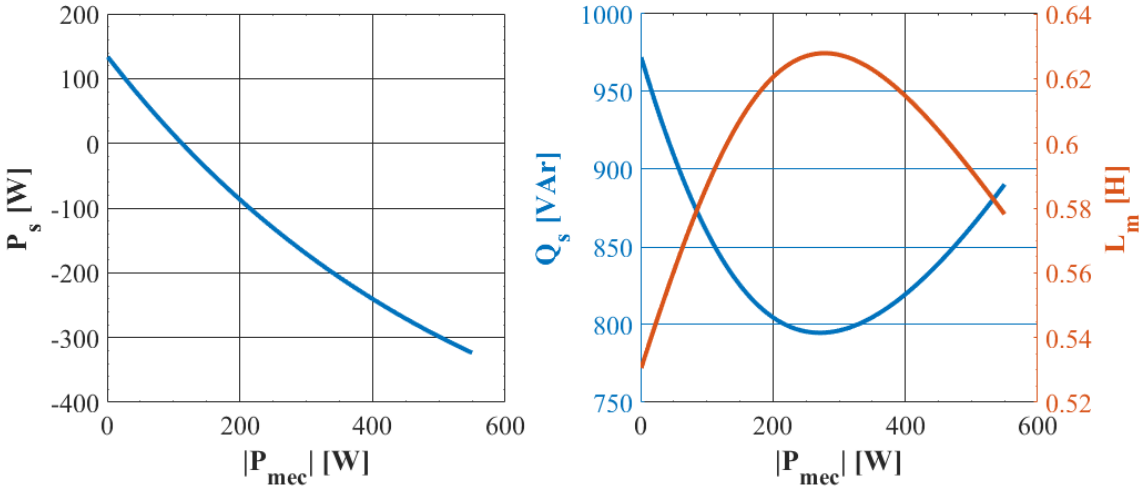

Figure 4.11: Ideal mechanical power control: stator active power (left) and reactive power / magnetizing inductance (right) as function of module of mechanical power.

4.3 Inverter based case

The inverter based case, as done in chapter three for speed control, is used to validate the ideal case of operation. Tests were performed for the nominal values of the machine ($5,78$ N m and 550 W). Figure 4.12 shows electromagnetic torque evolution and stator currents are depicted in Figure 4.13. Comparing the results with the ones obtained for the ideal case of operation, present in Figures 4.3 and 4.4, respectively, one sees that speed of convergence is the same, although when the inverter is feeding the machine quantities show oscillations because voltage has harmonics, as shown in Figure 4.14.

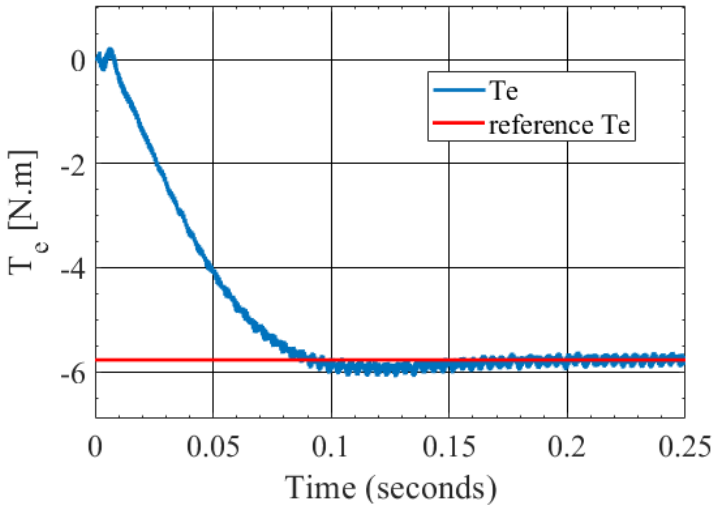

Figure 4.12: Inverter based case torque control: torque for P = 100, I = 100000 (current controllers).

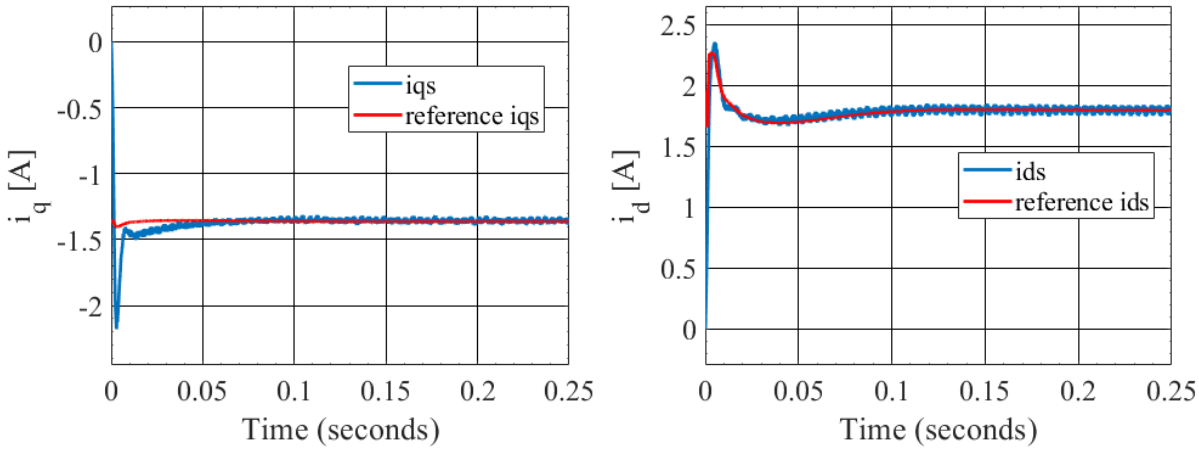

Figure 4.13: Inverter based case torque control: i_{qs} (left) and i_{ds} (right) currents for P = 100, I = 100000 (current controllers).

Figure 4.14 shows current and voltage evolution. As expected, current maintains a perfectly sinusoidal waveform, but voltage does not, as was seen in speed control (Figure 3.12). Figure 4.15 illustrates

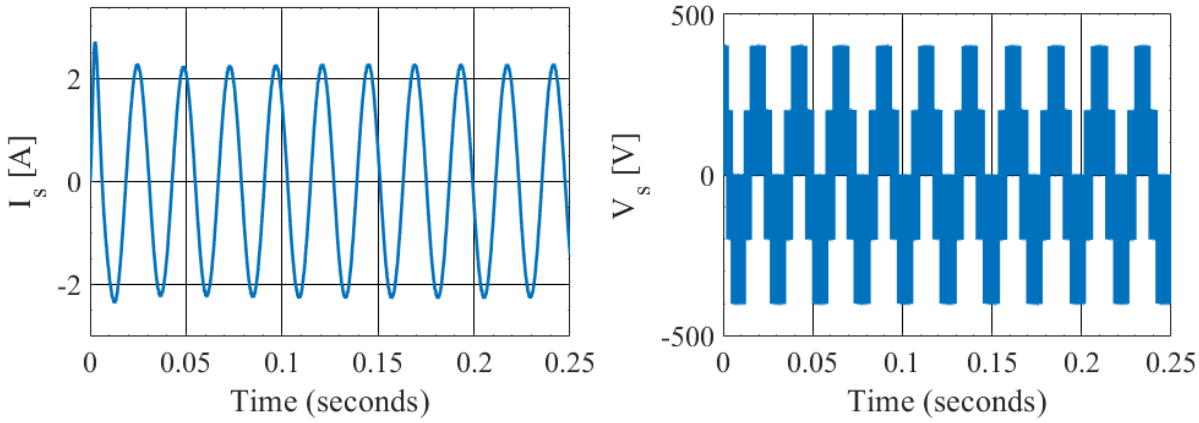

Figure 4.14: Inverter based case torque control: stator current (left) and single-phase voltage (right) for operation at rated torque.

mechanical power evolution and Figure 4.16 contains stator currents. Oscillations in the convergence region are present once more, but shape is the same as in Figures 4.8 and 4.9.

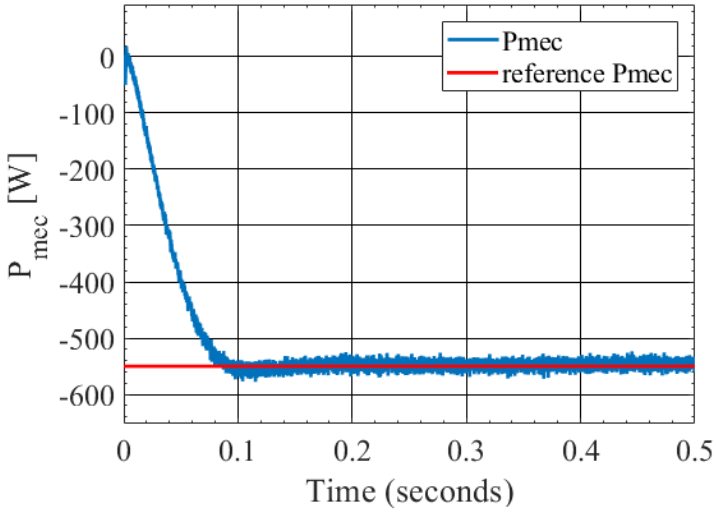

Figure 4.15: Inverter based case mechanical power control: mechanical power for P = 1000, I = 100000 (current controllers).

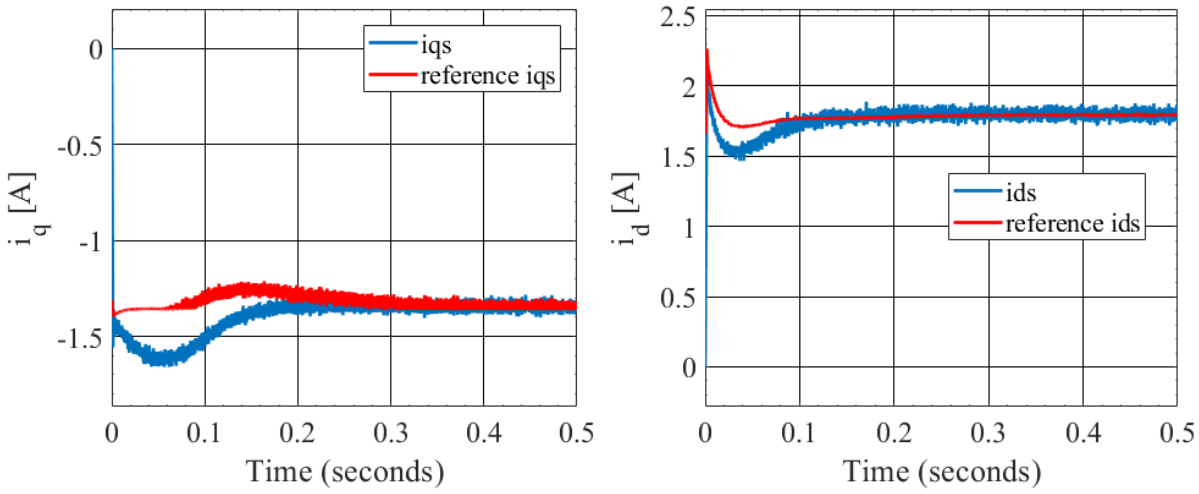

Figure 4.16: Inverter based case mechanical power control: i_{qs} (left) and i_{ds} (right) currents for P = 10, I = 1000 (torque controller) and P = 100, I = 100000 (current controllers).

4.4 Loss minimization in steady-state

Operating the machine at rated flux will be far from optimal in a variety of situations. Most of the time, the machine will operate in partial-load regime and run below its rated efficiency. To bypass this problem, the field-generating current and consequently the generated magnetic field needs to be reduced to an optimal level, allowing the same torque to be obtained with a lower stator current, resulting in lower ohmic and iron losses in the machine. In this section, the objective is to use a method to minimize the induction machine ohmic losses in steady-state operation.

From [11], the model of the machine losses, consisting of the ohmic losses in the stator and the rotor, neglecting iron losses, is as follows

$$P_{loss} = \frac{3}{2}\left(R_s + R_r\frac{L_m^2}{L_r^2}\right)\left(i_{ds}^2 + i_{qs}^2\right) - 3R_r\frac{L_m}{L_r^2}\lambda_{dr}i_{ds} + \frac{3}{2}\frac{R_r}{L_r^2}\lambda_{dr} \tag{4.4}$$

Iron losses have been neglected since the model used so far does not take the magnetizing resistance into account. Later, the influence of this parameter will be analyzed.

From section 3.3.1, the relation between the reference field-generating current i_{ds}^* and the reference rotor flux λ_{dr}^* is

$$i_{ds}^* = \frac{\lambda_{dr}^*}{L_m} \tag{4.5}$$

and the relation between the reference torque generating current i_{qs}^* and the reference electromagnetic torque T_e^* is

$$i_{qs}^{*} = \frac{2}{3}\frac{L_r T_e^{*}}{L_m p \lambda_{dr}^{*}}. \tag{4.6}$$

From the model (4.4), by substituting the currents (4.5) and (4.6), the optimal steady-state flux can be found by solving

$$\frac{\partial P_{loss}}{\partial \lambda_{dr}^{*}} = 0. \tag{4.7}$$

The optimal reference flux depends on torque and machine parameters and is given by

$$\lambda_{dr_{opt}}^{*} = \sqrt{\frac{2}{3}\frac{T_e^{*}}{p}}\left(\frac{R_s L_r^2 + R_r L_m^2}{R_s}\right)^{\frac{1}{4}} \tag{4.8}$$

The value of the flux to be applied to the machine will be limited to the rated value ($1,04$ Wb). Using the optimized flux, one can compute the necessary i_{qs}^{*} current to produce the desired reference torque T_e^{*} with the lowest possible copper losses in steady-state.

To verify the loss optimization method, tests were made for torque control. As seen, torque and mechanical power control are equivalent for a constant speed. The ideal case of operation was considered. The tests consist of simulating the machine's behaviour for a variety of torque reference values and computing its efficiency, assuming that the machine is running at its rated speed (910 rpm).

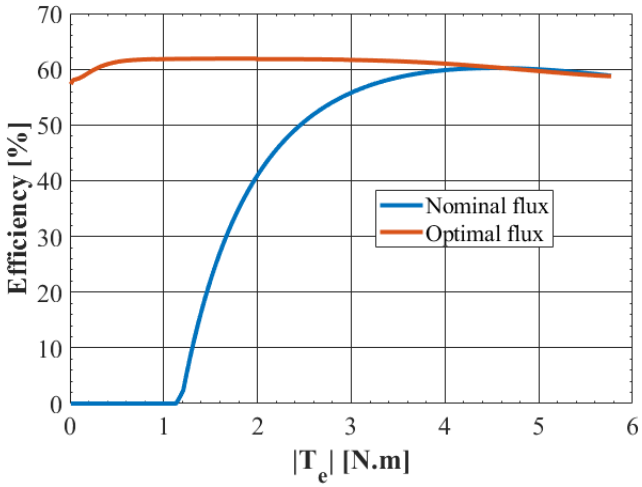

Figure 4.17: Induction machine efficiency as function of the module of electromagnetic torque for operation at rated speed (910 rpm).

Figure 4.17 shows that for low values of torque, the generator's efficiency is zero when the rated flux is used to calculate the field-generating current, as seen previously. This is because of the high stator and rotor resistances of the induction machine.

The results obtained for the operation at optimal flux are substantially better. Efficiency is now closer

to 60% throughout the entire range of reference values. The improvement of efficiency for lower torque values is notorious because now the machine is always operating in generator mode, meaning that it is supplying active power on the stator. For values closer to the nominal point of operation, one can conclude that the results are the same for operation at rated flux and optimal flux. Indeed, for higher values of torque, given that the speed of rotation is assumed to be constant, the optimal flux is approximately equal to the rated flux because it is proportional to the square root of the torque, as seen in Eq. (4.8). Figure 4.18 shows the evolution of optimal flux for different values of torque.

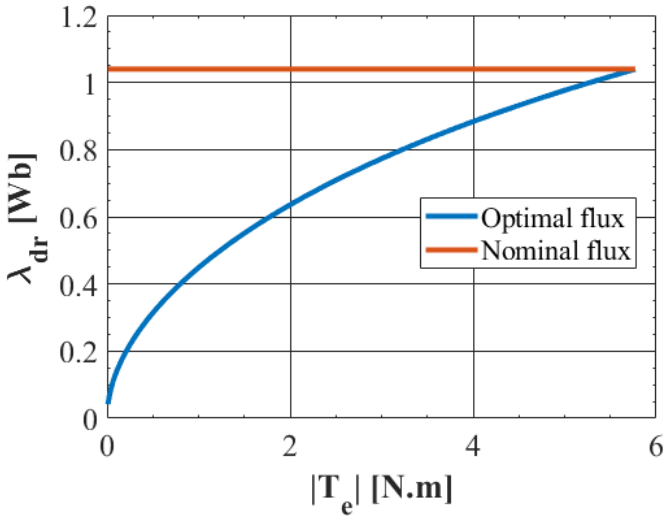

Figure 4.18: Rotor flux as function of the module of electromagnetic torque for operation at rated speed (910 rpm).

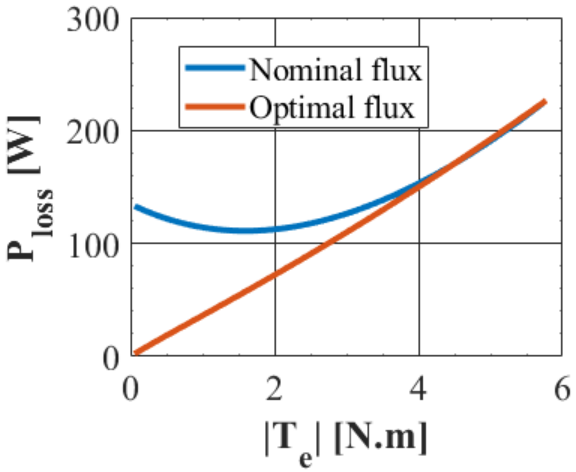

Figure 4.19: Power losses as function of the module of the electromagnetic torque for operation at rated speed (910 rpm).

Figure 4.19 confirms what has been concluded until this point. For low values of torque and mechanical power, losses are smaller than when using rated flux. For operation points near the nominal point,

the usage of optimal flux or rated flux will produce the same results simply because the closer one gets to the nominal point, the closer optimal flux and rated flux become.

A major conclusion from this loss optimization algorithm is that it is especially useful when the machine operates in a partial load regime. As shown in these situations, using the rated flux as a reference to produce the field-generating current i_{ds} is a very poor choice that leads to extremely inefficient use of the machine. Lowering the field-generating current and consuming reactive power is a good way to improve its performance.

5

Introduction of the Pump as Turbine in the generating system

Contents

5.1 Introduction

In this chapter, the inclusion of the pump as a turbine (PAT) in the system is studied. Its model has been completely developed in [9], so only the final equations will be presented here. When coupling the turbine to the induction generator, there are new variable quantities: water pressure and flow rate. In a real application, they are not constant and may experience sudden changes.

To understand how a change in pressure affects the system, simulations were performed for three turbine water pressures: 80%, 100% (or nominal pressure of 72100 Pa), and 120%. The simulations were performed using the ideal voltage case of operation (Figure 3.2 for speed control, Figure 4.1 for torque control and Figure 4.2 for mechanical power control). In these simulations, various mechanical power, torque, and speed reference values were used, as well as the loss optimization method for steady-state operation. As seen in the previous chapters, supplying the generator through a power inverter has produced the same results as those obtained for the ideal operation case. Besides this, using the ideal case of operation proved to be better in terms of processing time. The results obtained are for steady-state operation.

5.2 Model of the PAT

The PAT model has two inputs: water pressure *P* and the shaft speed of rotation N_r. The output that will impact the entire PAT-IG system is the mechanical torque produced by the PAT.

The first quantity being calculated is the head drop *H*, which is given by

$$H = \frac{P}{\rho g} \tag{5.1}$$

where ρ is the water density in $\mathrm{kg\,m^{-3}}$ and g the the gravitational constant in $\mathrm{m\,s^{-2}}$. Pressure *P* is in Pa and H in $m.w.c.$ The second quantity is flow rate *Q* ($\mathrm{m^3\,s^{-1}}$), which can be calculated through the PAT Q-H curves. These curves were experimentally determined in [5]. The curves were interpolated by a second-order polynomial, since it is a typical type of curve for a PAT, given by

$$H = \alpha^2 A + \alpha B Q + C Q^2, \tag{5.2}$$

where *A*, *B* and *C* are the polynomial coefficients and $\alpha = \frac{N_r}{N_{ref}}$. The coefficients and the reference speed N_{ref} were also obtained with experimental data and are: *A* = $3,6644$; *B* = $94,45$; *C* = 314560 and $N_{ref} = 1050$ rpm. These data can be used to predict the corresponding characteristics for other geometrically similar pumps under different operating points by applying the *similarity laws*.

From equation (5.2) one can compute the water flow

$$Q = \frac{-\alpha B \pm \sqrt{(\alpha B)^2 - 4C(\alpha^2 A - H)}}{2C} \tag{5.3}$$

The next step is to obtain the PAT efficiency. As done for flow rate *Q* with the Q-H curves, the efficiency curve as a function of rotational speed and the head drop was obtained experimentally. Interpolation of the experimental data resulted in the curve present in Figure 5.1.

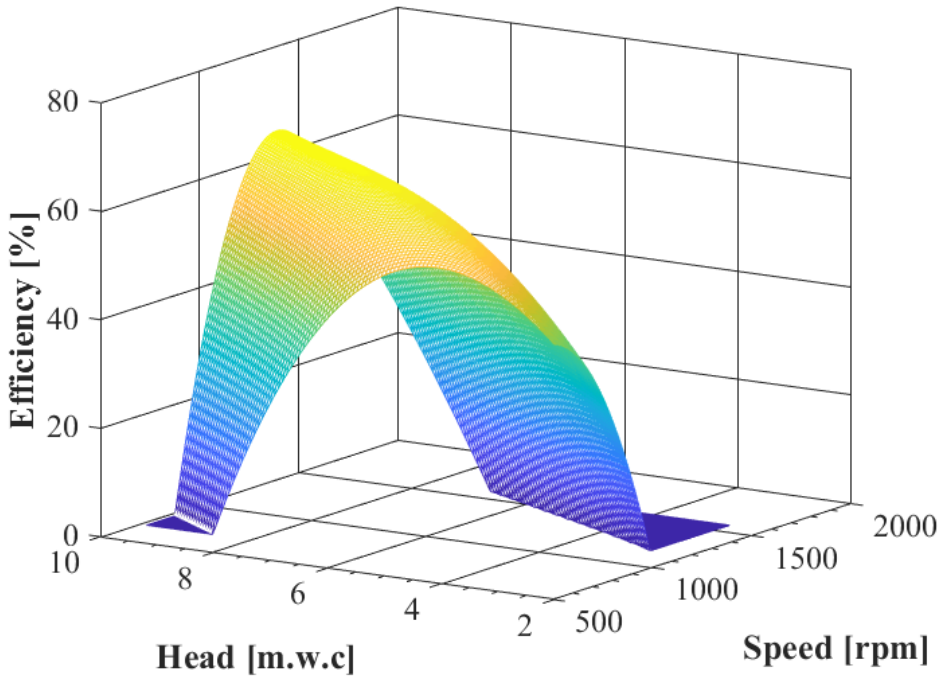

Figure 5.1: Efficiency curve of the PAT.

To complete the model, hydraulic power, hydraulic torque and mechanical torque have to be computed. The hydraulic power transferred to the shaft is given by

$$P_{hyd} = QP = \rho g Q H \tag{5.4}$$

Hydraulic torque can be calculated as

$$T_{hyd} = \frac{P_{hyd}}{w_m} = \frac{\rho g Q H}{w_m}, \; w_m = N_r \frac{2\pi}{60} \tag{5.5}$$

where w_m is the mechanical speed of rotation (in $\mathrm{rad\,s^{-1}}$), and the output mechanical torque on the pump shaft is given by

$$T_{mec_{PAT}} = T_{hyd}\eta_{PAT} = \frac{\rho g Q H}{w_m}\eta_{PAT} \tag{5.6}$$

The mechanical coupling equation of the system is

$$J\frac{dw_m}{dt} = T_{mec_{PAT}} + T_e - T_{losses} \tag{5.7}$$

Note that $T_{mec_{PAT}}$ is a positive value and T_e is a negative value because the induction machine is operating in generator mode. In steady-state, the PAT model must return the electromagnetic torque produced by the induction machine apart from losses.

The complete generating system model is present in Figure 5.2.

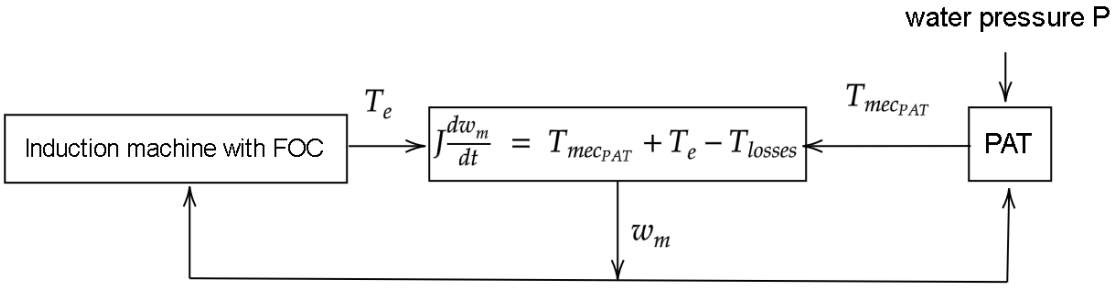

Figure 5.2: Complete generating system.

The generating unit efficiencies are as follows

$$\eta_{PAT} = \frac{P_{mec}}{P_{hyd}},\ \eta_{gen} = \frac{P_s}{P_{mec}},\ \eta_{global} = \eta_{PAT}\eta_{gen} \tag{5.8}$$

5.3 Numerical results of the control methods

5.3.1 Speed control

In [9], it was concluded that the machine did not maintain its frequency constant throughout the experiments. Speed control will allow control of the electrical frequency of all quantities. This type of control was firstly introduced in chapter three when developing the field-oriented control algorithm. It is now intended to see how the speed control algorithm performs when the PAT is coupled to the generator.

Figure 5.3 shows the PAT-generating unit global efficiency obtained as a function of the group speed when steady-state operation was reached. For a pressure of $80\ \%$ of the nominal one, maximum efficiency was $47\ \%$ for a speed of 1365 rpm. For the nominal pressure (72100 Pa), maximum efficiency was $49,7\ \%$ for a speed of 1505 rpm, and for $120\ \%$ of the nominal pressure, maximum efficiency was $49,8\ \%$ for a speed of 1715 rpm.

By observing Figure 5.3, the first conclusion is that the higher the pressure the higher the speed

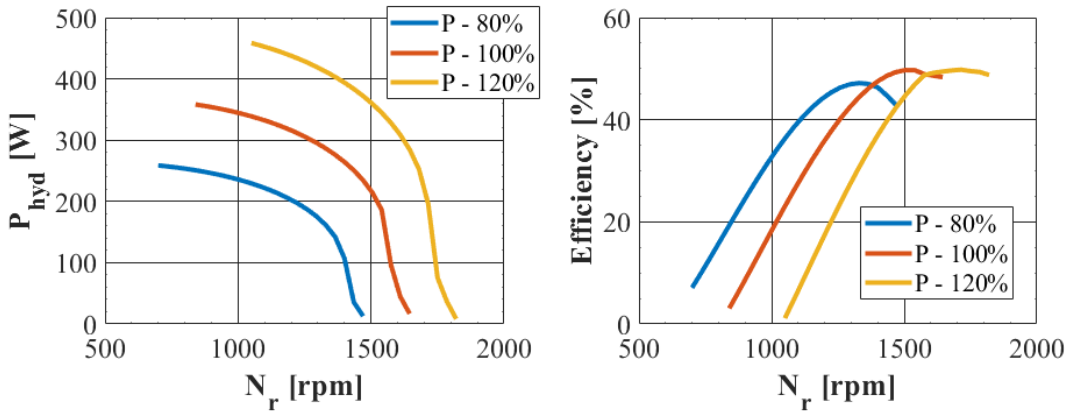

Figure 5.3: Speed control: hydraulic power (left) and global efficiency (right) as function of speed for operation at different water pressures.

needs to be to obtain the same efficiency. For instance, for a speed of 1000 rpm and pressure of 80 % efficiency is 33 %, but for the same speed with a pressure of 120 % the efficiency is not defined. By observing the results present in Figure 5.4 one concludes that the generator efficiency is pretty much the same for every pressure, but the PAT efficiency is not. That shows that PAT behaviour has the highest influence in global efficiency. Indeed, the generator has been optimized to perform at its best possible efficiency by decreasing the rotor flux to the optimal level, which minimizes losses despite the operating point.

On the other hand, the PAT operation point is completely defined by speed and pressure (that is constant), and there is no control of other hydraulic variables. The flow rate depends only on speed as seen in Eq. (5.3), as the head drop is a constant value that only depends on water pressure, which is assumed to be constant in each of the tests. Therefore, hydraulic power is also dependent on speed, as it is directly proportional to flow rate as shown in Eq. (5.4). Finally, PAT efficiency is a function of head drop and rotational speed. With a constant head drop, speed defines the operating point (Figure 5.1).

Figure 5.5 shows active power delivered in the generator stator and mechanical power in its shaft (in absolute values). As expected, the higher the pressure, the higher the maximum delivered power will be. Note that there is a peak where the output power is greatest and then starts decreasing. To understand why this happens, one can start by looking at the evolution of flow rate with speed present in Figure 5.7. As shown, the flow rate decreases as speed increases. Therefore, increasing speed will result in lower hydraulic power, but not in lower efficiencies as seen in Figures 5.3 and 5.4. That is why as speed increases, mechanical power and active power increase in the first stage (efficiencies increase at a faster rate than the rate of decrease of hydraulic power), but then start to decrease as efficiency stabilizes.

Figure 5.6 shows the evolution of electromagnetic torque. As expected, torque evolution has the

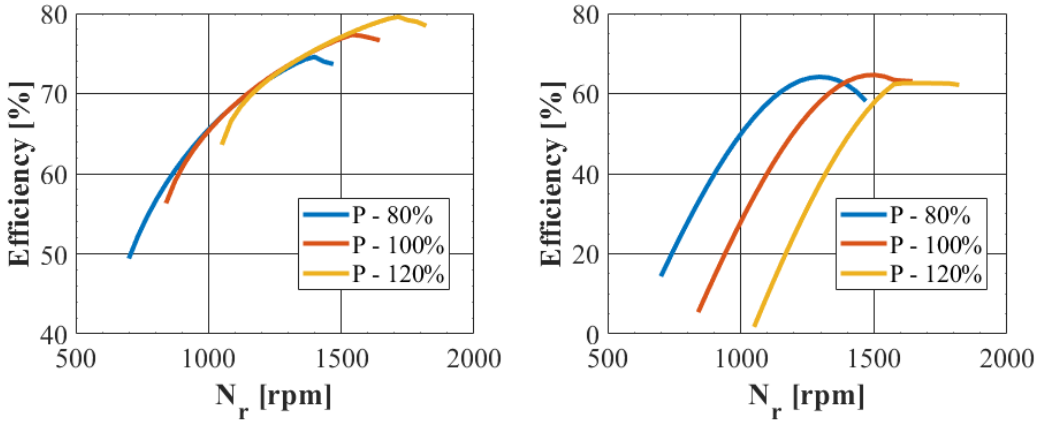

Figure 5.4: Speed control: Efficiencies of the generator (left) and PAT (right) as function of speed for operation at different water pressures.

same shape as mechanical power. Note that powers and torque are negative since the induction machine is operating as a generator, but for a better visualization they are shown in absolute value.

Figure 5.8 contains a 3-D representation of the curves present in Figure 5.5 for better visualization of how water pressure affects active power delivered in the stator. Table 5.1 contains the results for the maximum points registered in the curves present in Figure 5.5.

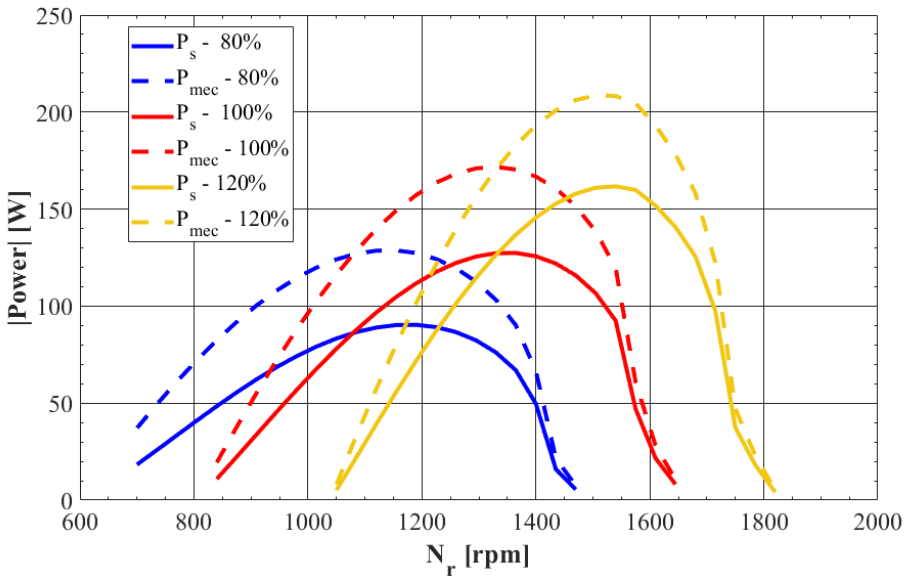

Figure 5.5: Speed control: stator active power (solid lines) and mechanical power (dashed lines) in absolute value as function of speed for operation at different water pressures.

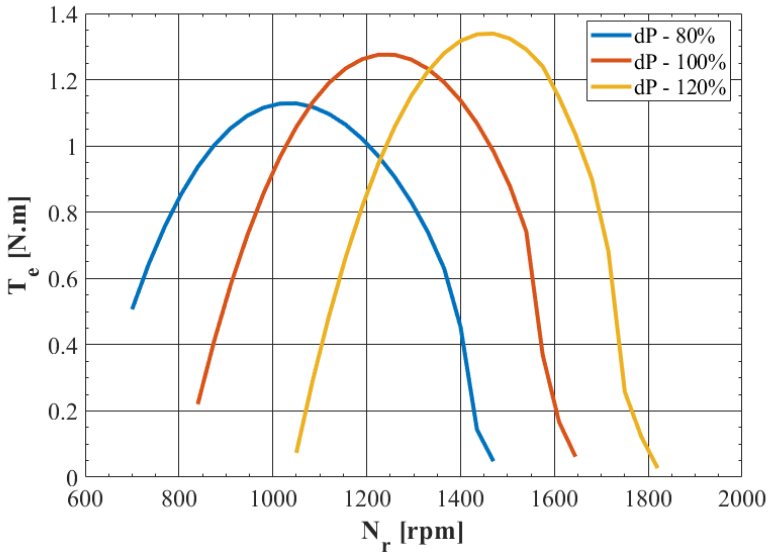

Figure 5.6: Speed control: electromagnetic torque produced by the generator in absolute value as function of speed for operation at different water pressures.

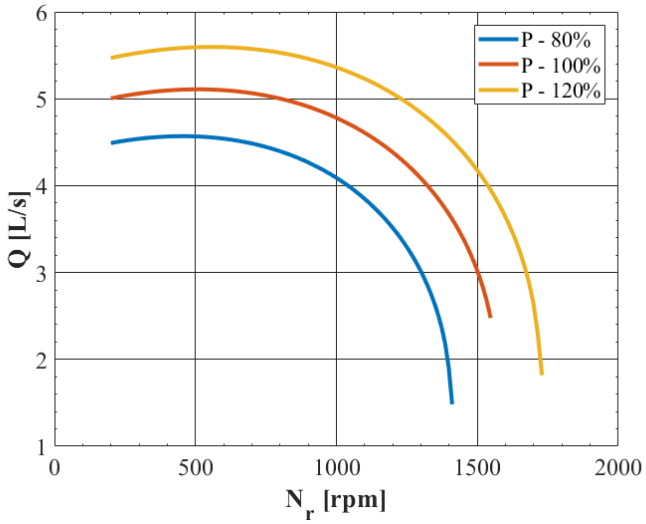

Figure 5.7: PAT flow rate as function of speed for different water pressures.

Table 5.1: Maximum active and mechanical powers obtained for speed control of the generating unit.

Pressure (p.u)	Max. P_s [W]	Max. P_{mec} [W]	η_{gen} [%]	η_{PAT} [%]	η_{global} [%]	N_r [rpm]	Q [l s^{-1}]
80 %	-90,35	-127,33	70,95	62,15	44,1	1190	3,55
100 %	-127,39	-170,4	74,76	61,7	46,13	1365	3,83
120 %	-161,73	-208,27	77,66	60,4	46,9	1540	3,99

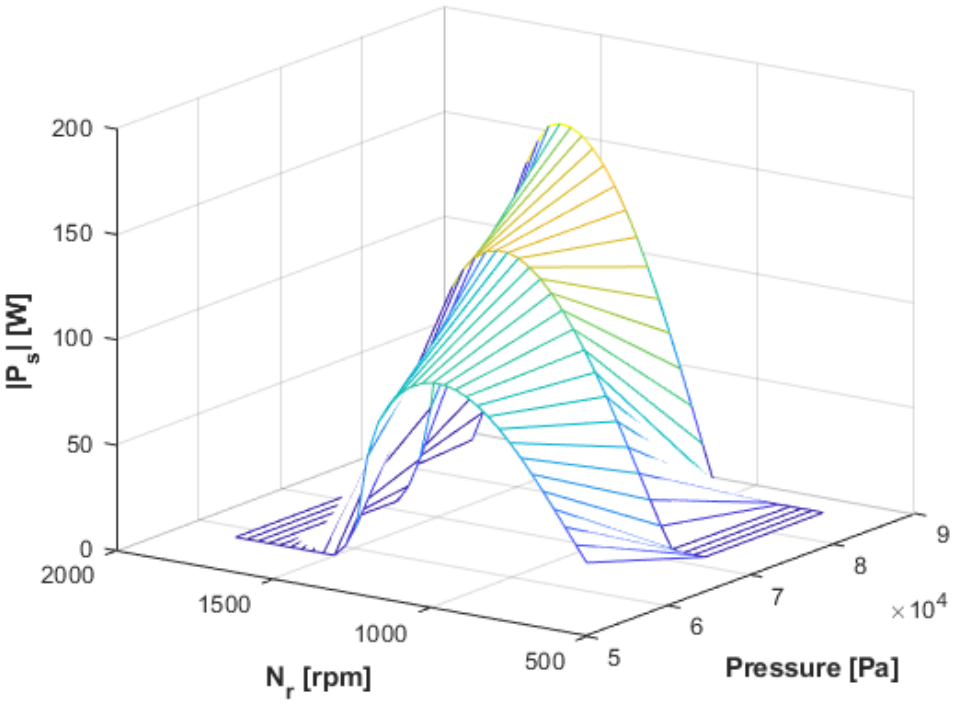

Figure 5.8: Speed control: stator active power in absolute value as function of speed and water pressure.

5.3.2 Mechanical power control

The results present in Figure 5.5 show that the maximum mechanical power on the shaft is lower than the induction machine nominal power of 550 W. This way, there is no need to test reference mechanical power values closer to the generator's nominal point of operation.

The results obtained for the speed of rotation and flow rate of the PAT are present in Figure 5.9. By observing Figure 5.9 it can be concluded that lower pressures lead to lower speeds as expected, but to higher flow rates of the PAT for the same mechanical power on its shaft. This result is following what was seen when performing speed control. However, hydraulic power does not seem to depend on pressure (Figure 5.10), although equation (5.4) shows that hydraulic power and pressure are directly related. The only explanation for it is that the flow rate decreases as pressure increases for the same amount of mechanical power, which is exactly what is happening (Figure 5.9).

Generator and PAT efficiencies are depicted in Figure 5.11. Higher pressures result in higher generator efficiency since speed is higher, resulting in lower optimal rotor flux and losses. PAT efficiency results from the combination of head drop and speed, as seen in Figure 5.1.

Finally, stator active power is represented in Figure 5.12. It can be seen that it is kept constant independently of pressure. This makes sense since one controls mechanical power and the generator efficiency has variations smaller than 3% for the entire range of operation. This being said, it can be

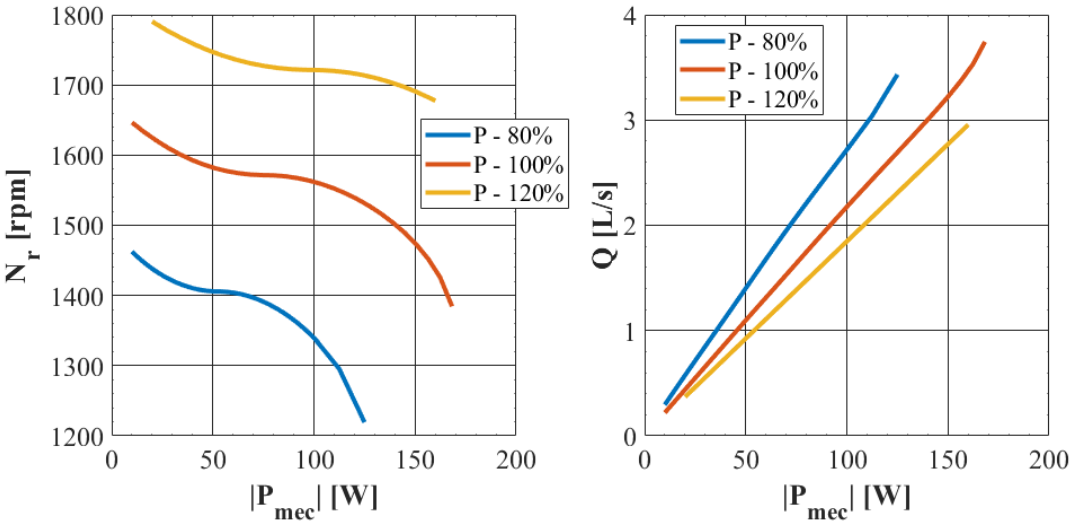

Figure 5.9: Speed of rotation (left) and flow rate (right) as function of module of mechanical power.

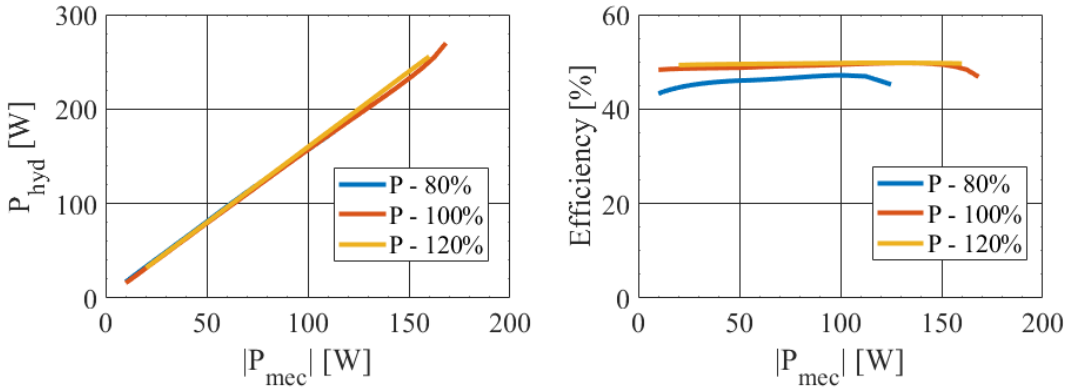

Figure 5.10: Hydraulic power (left) and global efficiency (right) as function of absolute value of mechanical power for operation at rated water pressure (72100 Pa).

concluded that mechanical power control allows one to supply the load with constant active power, even though water pressure changes.

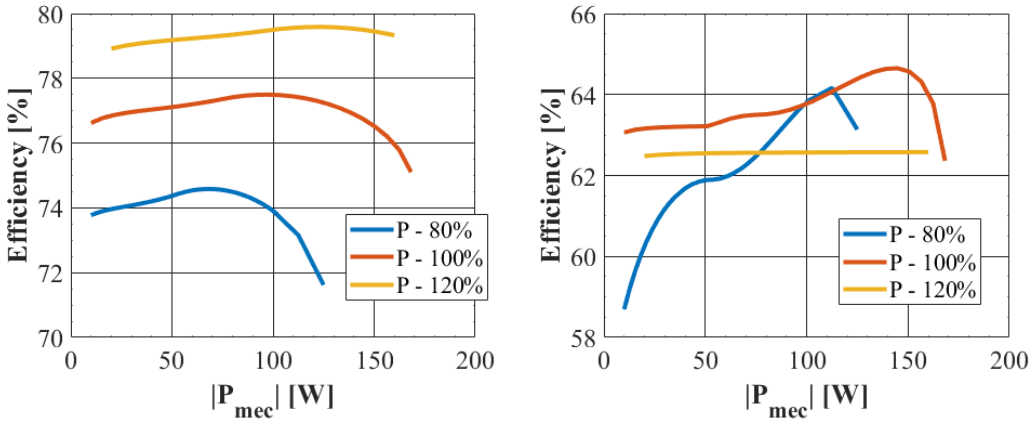

Figure 5.11: Mechanical power control: generator efficiency (left) and PAT efficiency (right) as function of absolute value of mechanical power.

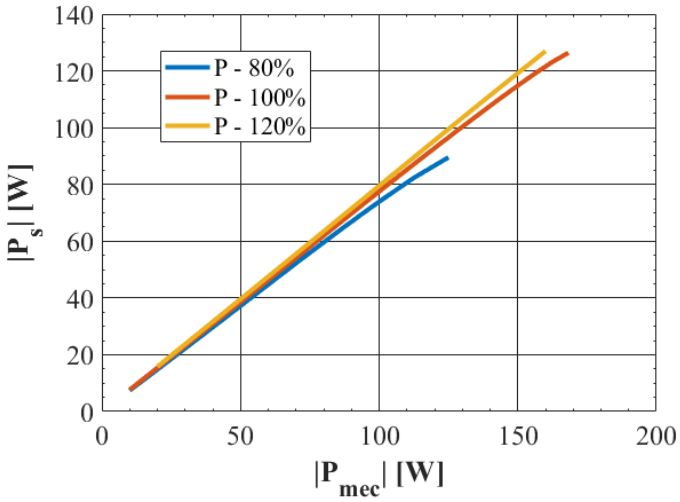

Figure 5.12: Mechanical power control: stator active power as function of absolute value of mechanical power.

5.3.3 Electromagnetic torque control

The same tests done for mechanical power control were performed for various reference values of electromagnetic torque. Figure 5.6 shows that torque has the same evolution as mechanical power. In fact, the maximum controllable torque is close to -1 N m, which is very small compared to the generator nominal torque of $-5,78$ N m.

Figure 5.13 shows group speed as function of torque. Once again, as the generator's nominal point of operation is not reached, there is no need to use torque values close to the nominal one. Figure 5.14 represents hydraulic power and global efficiency of the generating unit. Hydraulic power increases as torque increases, since a higher torque means higher mechanical power and therefore a higher hydraulic power because efficiencies do not change drastically throughout the entire range of torque values. Figure 5.15 shows the generator and PAT efficiencies.

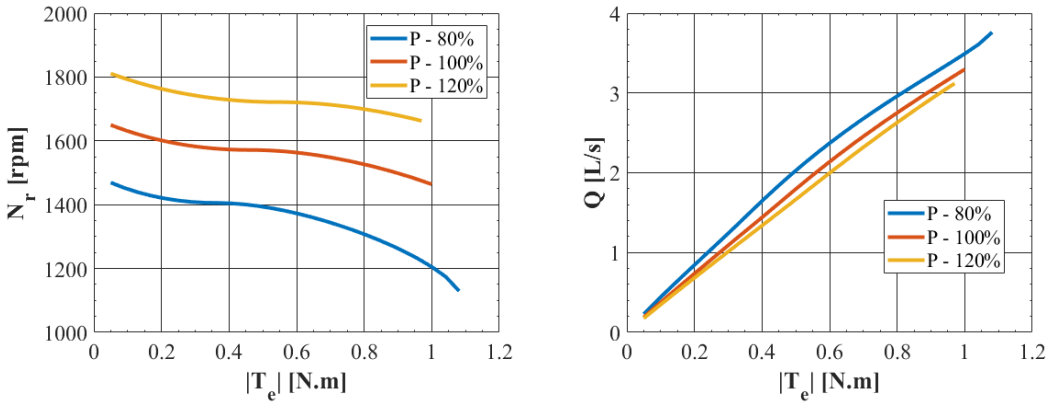

Figure 5.13: Torque control: speed (left) and flow rate (right) as function of of absolute value of electromagnetic torque.

When controlling electromagnetic torque, one cannot supply the load at constant active power, which was possible when controlling mechanical power. Depending on the pressure, the same torque value will result in a different mechanical power on the shaft (different speed) and consequently a different active power on the generator stator, as seen in Figure 5.16.

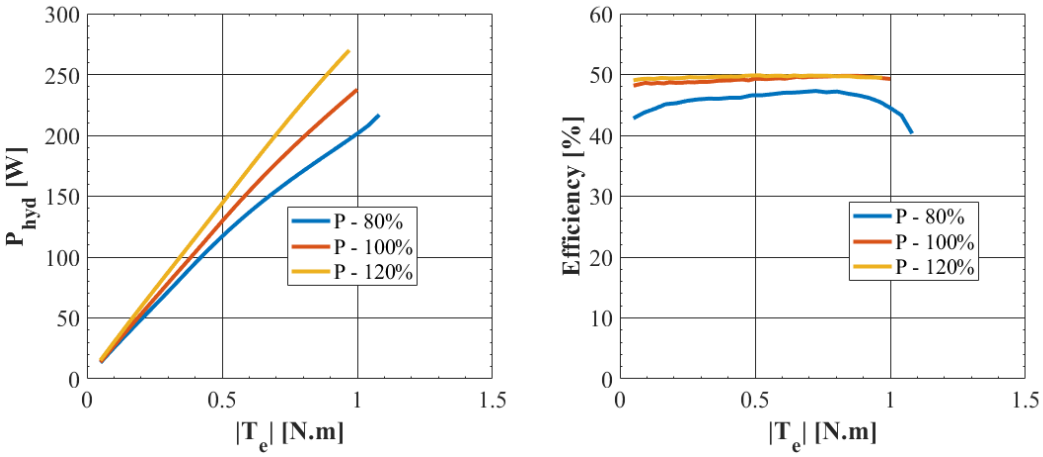

Figure 5.14: Torque control: hydraulic power (left) and global efficiency (right) as function of absolute value of electromagnetic torque.

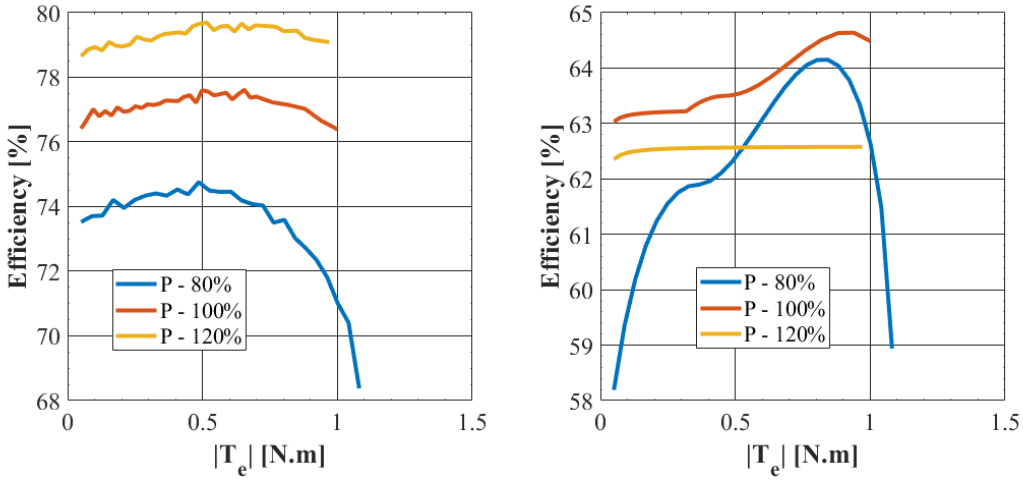

Figure 5.15: Torque control: generator (left) and PAT efficiencies (right) as function of absolute value of electromagnetic torque.

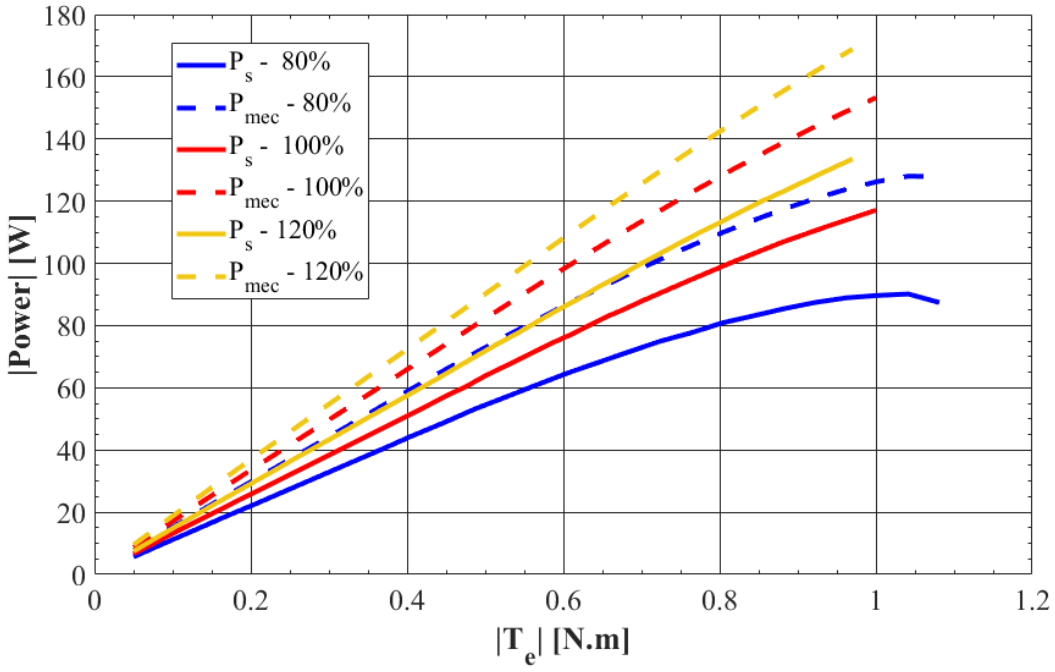

Figure 5.16: Torque control: stator active power (solid lines) and mechanical power (dashed lines) as function of absolute value of electromagnetic torque for operation at different water pressures.

5.3.4 Conclusion

The shape of the power curves present in Figure 5.5 and of torque in Figure 5.6, obtained for speed control, show that mechanical power and torque control are not the most reliable way of controlling the system. For instance, by observing Figure 5.12 one sees that, for operation at 80% of rated water, the maximum controllable mechanical power was -120 W (blue line), whereas by looking at Figure 5.5 the maximum mechanical power obtained pressure was -135 W (blue dashed line). In mechanical power control, it was observed that if the reference value kept increasing above -120 W the system started to become unstable and could no longer be controlled because the closer one gets to the maximum possible value, the closer the two possible points of operation are, i.e., their corresponding speeds are less far apart, as illustrated in Figure 5.5.

Speed control of the generating unit was useful because it showed that the other types of control - mechanical power and torque - are not reliable if they don't consider the group's rotational speed. As seen, there are two possible points of operation for the system for the same value of power or torque. Therefore, without a reference speed, they can't be distinguished. The results obtained for mechanical power control and torque control (Figures 5.9 and 5.13, respectively) showed that the system ended up operating in the highest speed points rather than in the lower speed points, which is the region with highest global efficiency. This is a good outcome, since in a real application it would be wise to choose

the point of operation where the generating unit efficiency is higher.

The most important conclusion regarding mechanical power control is that it allows one to supply the load with constant active power, even though water pressure changes. In torque control, this is not possible, as shown in Figure 5.16. In terms of efficiency, this two types of control will put the system operating at a pretty much constant efficiency for the entire range of reference values, as shown in Figure 5.10 and 5.14.

When performing speed control, the PAT will have very different operation points, so its efficiency (and consequently global efficiency) will assume a wider range of values (Figure 5.4) than in mechanical power and torque control (Figures 5.11 and 5.15, respectively). The generator efficiency has been optimized by applying the loss minimization method to reduce rotor flux, so it does not have much influence in the generating unit global efficiency regardless of the control type used.

6

Inclusion of the magnetizing resistance in the machine model

Contents

6.1 Introduction

In this chapter, the inclusion of the magnetizing resistance in the induction machine model is studied. This resistance will introduce further losses in the generator (iron losses), so the expected result is a decrease of efficiency. Firstly, this parameter is described and the field-oriented control algorithm with the loss minimization method is rearranged. Then, tests for electromagnetic torque and mechanical power controls are performed, being compared to those obtained in chapter four for the stand-alone generator operation. In the end, speed control of the generating unit was performed.

6.2 Induction machine model

The introduction of the magnetizing resistance R_m changes the fluxes equations a shown in [12]. They are as follows

$$\lambda_{ds} = L_s i_{ds} + L_m i_{dr} - \frac{L_s}{R_m}\left(\frac{d\lambda_{ds}}{dt} - w_s \lambda_{qs}\right) \tag{6.1}$$

$$\lambda_{qs} = L_s i_{qs} + L_m i_{qr} - \frac{L_s}{R_m}\left(\frac{d\lambda_{qs}}{dt} + w_s \lambda_{ds}\right) \tag{6.2}$$

$$\lambda_{dr} = L_r i_{dr} + L_m i_{ds} - \frac{L_m}{R_m}\left(\frac{d\lambda_{ds}}{dt} - w_s \lambda_{qs}\right) \tag{6.3}$$

$$\lambda_{qr} = L_r i_{qr} + L_m i_{qs} - \frac{L_m}{R_m}\left(\frac{d\lambda_{qs}}{dt} + w_s \lambda_{ds}\right) \tag{6.4}$$

The voltages equations are the same (Eqs.(3.3) to (3.6)). This change in the flux equations mean that the field-oriented control algorithm has to be re-deduced. The principle behind the deduction is still the same though ($\lambda_{qr} = 0$). From Eq.(3.5), in steady-state, making $\lambda_{qr} = 0$, one directly obtains

$$i_{dr} = 0 \tag{6.5}$$

Substituting this result in Eq. (6.3) one gets in steady-state

$$\lambda_{dr} = L_m i_{ds} + \frac{L_m}{R_m} w_s \lambda_{qs} \tag{6.6}$$

Solving Eq.(6.4) for i_{qr} gives

$$i_{qr} = -\frac{1}{L_r}\left(\frac{L_m}{R_m} w_s \lambda_{ds} - L_m i_{ds}\right). \tag{6.7}$$

Solving Eq.(3.6) results in

$$w_r = -R_r \frac{i_{qr}}{\lambda_{dr}} \tag{6.8}$$

Substituting Eqs.(6.6) and (6.7) in Eq.(6.8) and applying the result to Eq.(3.1) gives

$$w_s = w_{me} - \frac{R_r}{L_r} \frac{w_s \lambda_{ds} - R_m i_{qs}}{w_s \lambda_{qs} + R_m i_{ds}}. \tag{6.9}$$

Integrating w_s one obtains the estimation of the electrical position of the rotating magnetic field concerning the stator geometry position, that is θ_s, that will be used to convert the *dq* quantities into the three phase *abc* quantities

$$\theta_s = \int w_s \, dt = \int \left(w_{me} - \frac{R_r}{L_r} \frac{w_s \lambda_{ds} - R_m i_{qs}}{w_s \lambda_{qs} + R_m i_{ds}} \right) dt \tag{6.10}$$

To calculate w_s one also needs to define the reference stator currents in the *dq* reference frame. Knowing that $i_{dr} = 0$, substituting in Eq.(6.3) gives the reference direct axis stator current

$$i_{ds}^* = \frac{1}{L_m} \left(\lambda_{dr}^* - \frac{w_s \lambda_{qs}}{R_m} \right). \tag{6.11}$$

To calculate the reference quadrature stator current, one will use the electromagnetic torque formula

$$T_e = \frac{3}{2} \frac{p}{2} \frac{L_m}{L_r} \lambda_{dr} (i_{qs} - i_{qs_{Fe}}), \tag{6.12}$$

that can be written as

$$i_{qs}^* = \frac{2}{3} \frac{2}{p} \frac{L_r}{L_m} \frac{T_e^*}{\lambda_{dr}^*} + i_{qs_{Fe}}. \tag{6.13}$$

Current $i_{qs_{Fe}}$ is the current that flows through the magnetizing resistance and, in steady-state, is given by

$$i_{qs_{Fe}} = \frac{v_{qs} - R_s i_{qs}}{R_m} \tag{6.14}$$

The magnetizing resistance will be calculated based on experimental data obtained previously in [8]. The curves of the R_m/f ratio and the flux image E/f obtained in this work are present in Figure 6.1. As done for the magnetizing inductance L_m, to obtain an expression to calculate R_m, these curves were interpolated using a second-order polynomial. The curve for 50 Hz was used since it is the machine's nominal frequency. The result obtained was

$$\frac{R_m}{f} = -2.5635 \left(\frac{E}{f} \right)^2 + 20.7288 \left(\frac{E}{f} \right) - 7.845 \tag{6.15}$$

To obtain the value of R_m the last step is to multiply the ratio R_m/f by the frequency f, given by

$$f = \frac{w_s}{2\pi} \tag{6.16}$$

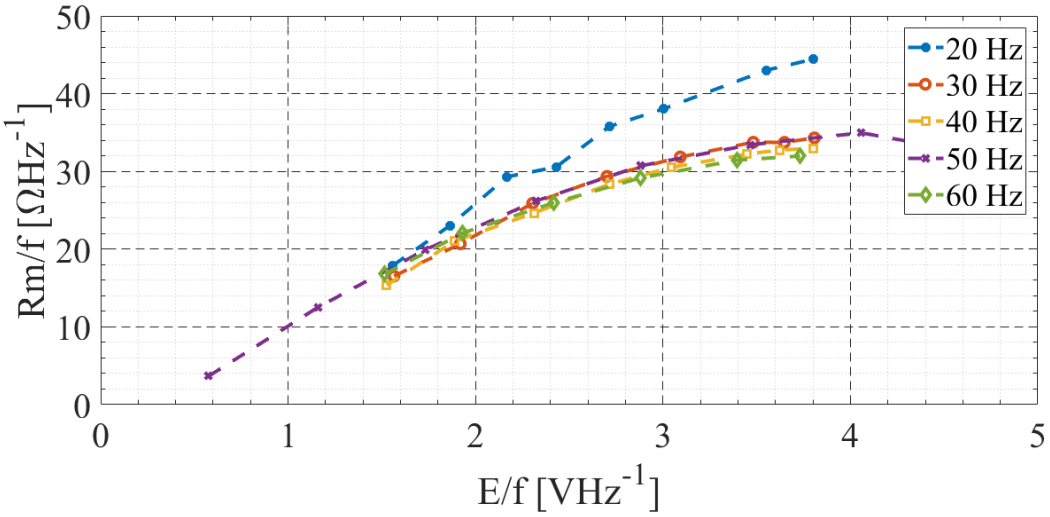

Figure 6.1: Evolution of R_m/f ratio as function of E/f from [8].

6.3 Loss minimization method

When including the magnetizing resistance R_m in the machine model, the power losses expression as present in [11] becomes

$$P_{loss} = \frac{3}{2}\left(R_s + R_r\frac{L_m^2}{L_r^2}\right)(i_{ds}^2 + i_{qs}^2) - 3R_r\frac{L_m}{L_r^2}\lambda_{dr}i_{ds} + \frac{3}{2}\left(\frac{R_r}{L_r^2} + p^2w_m^2\frac{L_m^2}{L_r^2R_m}\right)\lambda_{dr}^2 \tag{6.17}$$

The optimal steady-state flux can be found by solving

$$\frac{\partial P_{loss}}{\partial \lambda_{dr}} = 0 \tag{6.18}$$

which gives

$$\lambda_{dr_{opt}}^* = \sqrt{\frac{2}{3}\frac{T_e^*}{p}}\left(\frac{R_sL_r^2 + R_rL_m^2}{R_sL_r^2 + L_m^4\frac{p^2w_m^2}{R_m}}\right)^{\frac{1}{4}} \tag{6.19}$$

Figure 6.2 shows how optimal flux changes when the magnetizing resistance is included in the model. It can be concluded that the inclusion of R_m decreases optimal flux. This makes sense since R_m introduces more losses in the generator, so the algorithm will reduce the flux to minimize those extra

losses. As will be seen ahead, using nominal flux resulted in a very poor performance.

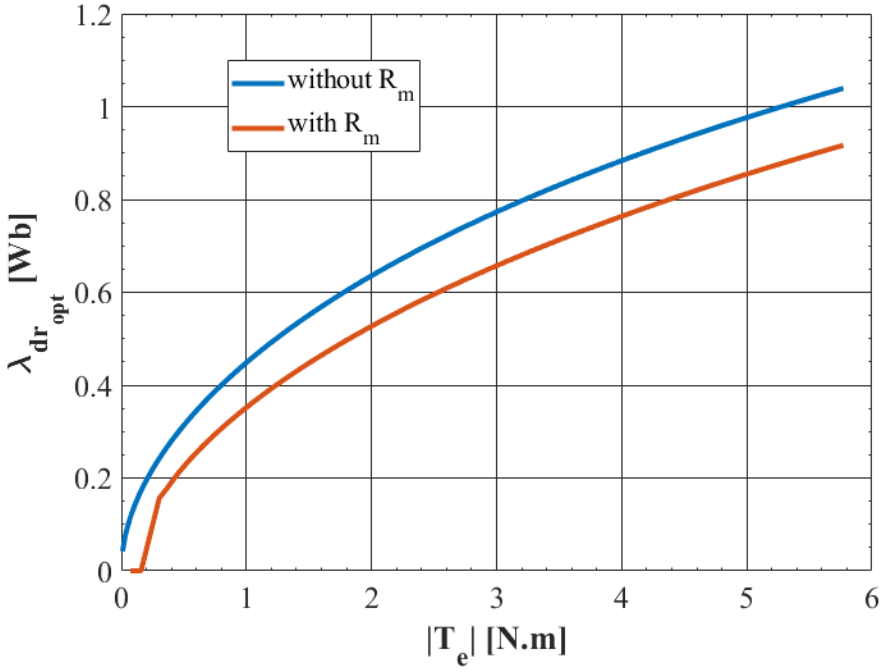

Figure 6.2: Optimal flux as function of absolute value of torque - comparison between results with and without magnetizing resistance for stand-alone operation.

6.4 Electromagnetic torque, mechanical power and speed control

As done in chapter four, simulations for various reference values of the two control variables (torque and mechanical power) were performed, assuming constant speed of rotation equal to the rated speed (910 rpm). Figures 6.3 and 6.4 show the machine efficiency as function of the referred variables. The results present in Figures 4.6 and 4.10 were included to compare the results obtained with the magnetizing resistance. As expected, efficiency drops overall when including this parameter in the model. The maximum efficiency obtained now was $48\ \%$ for an electromagnetic torque of -4 N m and a mechanical power of -384 W, whereas before this value was $60,2\ \%$, showing a decrease of $20\ \%$ when using optimal flux. Nominal flux proved to be an extremely poor choice, since the machine cannot operate in generator mode for almost the entire range of reference values.

The results present in Figures 6.5 and 6.6 show how power losses change as a function of torque and mechanical power, respectively. Comparing the results with the ones obtained in chapter four one concludes that the power losses increase when taking R_m into account, as expected. Using nominal flux results in a very poor performance as seen previously, and that conclusion is even more obvious

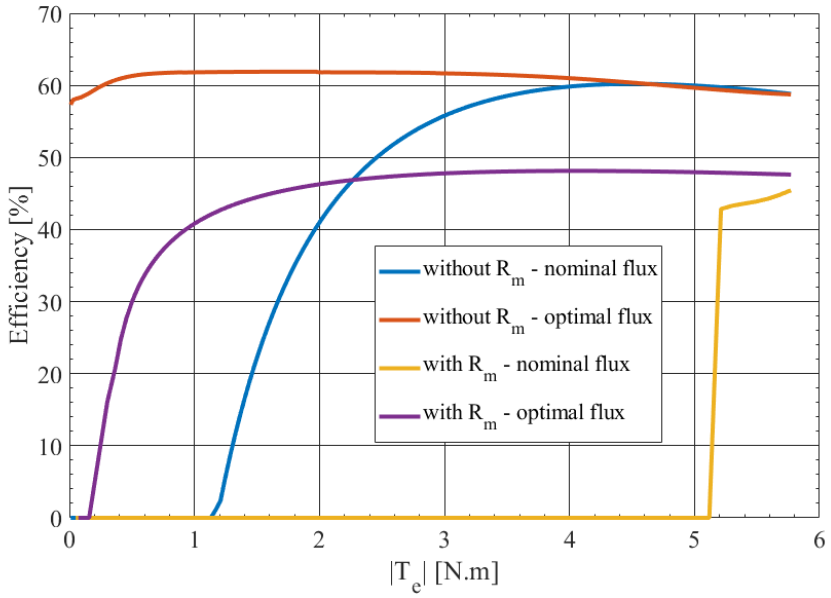

Figure 6.3: Ideal torque control: induction machine efficiency as function of absolute value of torque - comparison between results with and without magnetizing resistance for stand-alone operation.

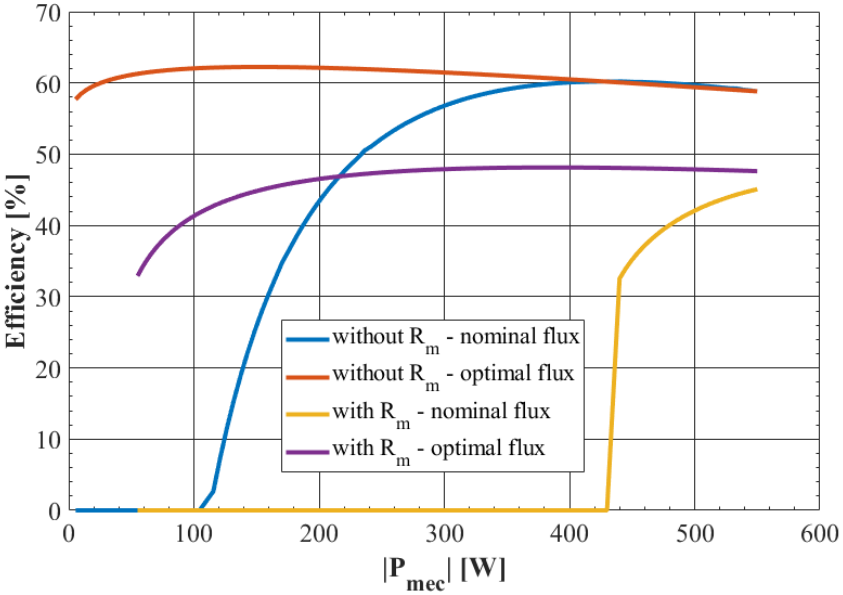

Figure 6.4: Ideal mechanical power control: induction machine efficiency as function of absolute value of mechanical power - comparison between results with and without magnetizing resistance for stand-alone operation.

when R_m is present in the model. The difference is most notorious in partial load regimes, which is to say for lower torque and mechanical power values, where the inclusion of R_m has proven to increase losses very significantly. The reason is that the machine will operate as a motor instead of a generator for a much wider range of reference values when R_m is considered. In fact, by looking at the efficiencies present in Figures 6.3 and 6.4 one can see that, for nominal flux usage, efficiency is zero for a much wider range of torque and power values. The sudden drop in power losses seen for nominal flux usage (yellow line) happens because the machine starts operate as generator at that exact point. Until this point, mechanical power on the shaft was not high enough to compensate the losses (at rated speed).

On the other hand, the use of the loss minimization method provided good results once more. With this method, even though losses are higher than when neglecting the magnetizing resistance, the increase is not as significant as when the nominal flux is used (50W on average of extra losses in this case).

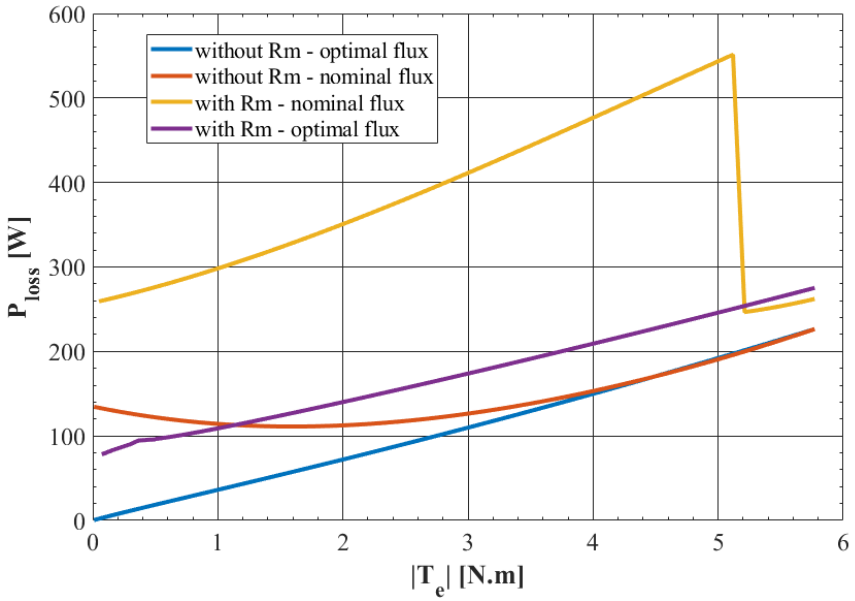

Figure 6.5: Ideal torque control: power losses as function of absolute value of torque - comparison between results with and without magnetizing resistance for stand-alone operation.

Finally, speed control was performed. Global efficiencies evolution as a function of speed are shown in Figure 6.7. The results present in Figure 5.3 were included for comparison. Table 6.1 contains the differences between the top efficiencies obtained for both scenarios.

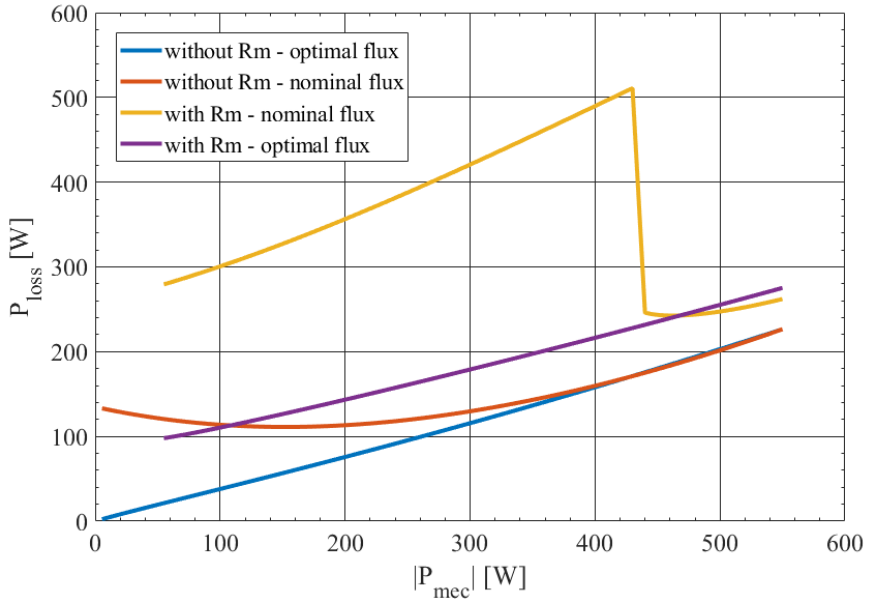

Figure 6.6: Ideal mechanical power control: power losses as function of absolute value of mechanical power - comparison between results with and without magnetizing resistance for stand-alone operation.

Table 6.1: Top efficiencies obtained for both scenarios - with and without iron losses - and respective deviation when performing speed control of the generating unit.

Scenario	Top efficiency without R_m [%]	Top efficiency with R_m [%]	Difference [%]
Pressure = 80%	47,2	32,8	30,5
Pressure = 100%	49,7	36,4	26,8
Pressure = 120%	49,8	37,5	24,7

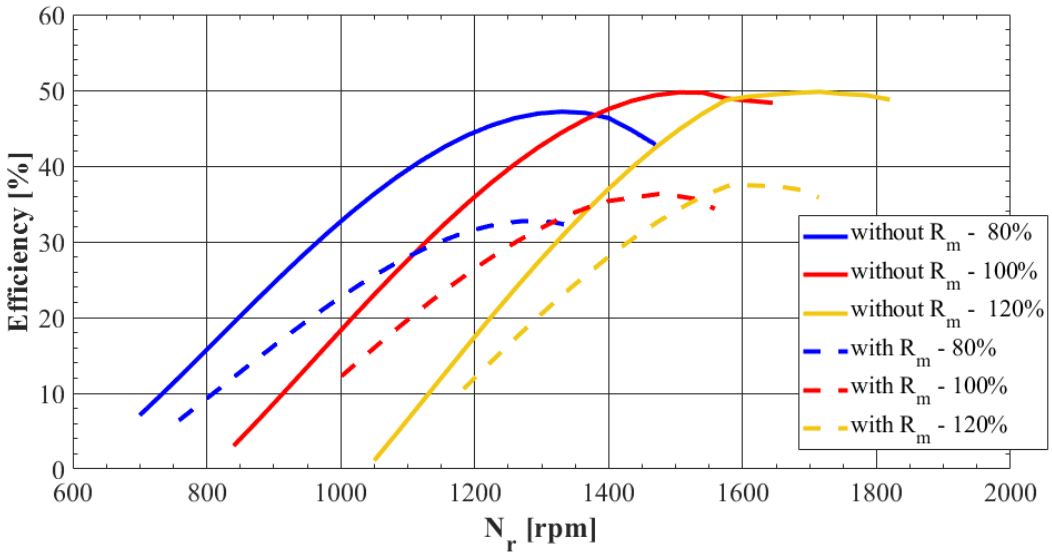

Figure 6.7: Speed control of the generating unit: comparison between global efficiencies obtained with and without iron losses.

7

Conclusion

Contents

7.1 Conclusions

As proposed, the field-oriented control algorithm was developed and tested for both the stand-alone generator operation and coupled to the PAT in steady-state regime. For the stand-alone operation, the control algorithm was initially designed for speed control, both when considering ideal voltages and when an inverter is supplying the induction machine.

The algorithm was then changed to allow electromagnetic torque and mechanical power control and tested for both cases. In these simulations, it was concluded that the generator efficiency was especially low in the partial-load regime, as the rated flux was imposed. Following these results, a method for optimizing the machine flux in steady-state operation was applied. It was seen that optimal flux, which is the one that minimizes losses, changes for each value of electromagnetic torque. When the machine is operating with optimal flux, the results showed a very significant improvement in the partial-load regime, with the generator efficiency being nearly constant and approximately equal to $60\ \%$ for all points of operation of the machine at rated speed (910 rpm).

Then, the PAT was coupled to the generator with the field-oriented control algorithm and the loss minimization method. Further tests were performed to evaluate the generating unit behaviour under control conditions. Speed control results were most revealing. They showed that the machine will have different operating points in terms of speed but will be supplying the load on the generator stator with the same active power. This means that a single control variable is not enough to impose the operating system point when performing either electromagnetic torque or mechanical power control, since there are two possible points of operation. It was seen that when imposing only torque or mechanical power, the system ended up operating in the higher speed points rather than the lower speed points of operation. Besides, when trying to impose torque and mechanical power values close to the maximum obtained for speed control, the system started to become unstable. As one gets closer to those maximum values, the two possible operating points get nearer, meaning that they are very similar, so the system cannot know the desired operating point. Fortunately, it operated at a higher global efficiency points. However, since these points have higher corresponding speeds, it may not be of interest for the system to operate in this region. It is also important to mention that the generator operated always in partial-load regime when coupled to the PAT, as its nominal point of operation was never reached.

In the end, the magnetizing resistance was included in the induction machine model to evaluate stand-alone operation efficiency and global efficiency when coupled to the PAT. The results showed that efficiency decreased around 20% in stand-alone operation and $25 - 30\%$ coupled to the PAT when iron losses were considered. The influence of R_m is high because the study was done for a low power induction machine. This influence becomes smaller for higher power machines.

7.2 System limitations and future work

As mentioned earlier, electromagnetic torque and mechanical power of the generating unit are not the most reliable way of control since there is redundancy in speed. Therefore, it is suggested to implement such control schemes considering the group speed of rotation instead of only torque or power. The generator has been optimized to obtain the best possible efficiency at all operation points by controlling its rotor flux. However, the PAT has been coupled to the generator and no control and/or optimization of hydraulic variables has been done. Besides this, the pump as a turbine being used so far in the studies is a low power PAT. As seen, the generator's nominal point of operation was never reached under any control method, so a higher power PAT may be suitable. These are pertinent topics to be studied in the future.

The transient regime has also not been studied in this thesis. When inputs change, the control algorithm's behaviour is very important to understand its reliability, especially in real applications.

At last, multiple PAT connections were not analyzed. Work on this subject has already been done in [9] though. This way, implementing the control algorithms developed in this thesis to associations of PATs instead of a single PAT and see how perturbations in one of the systems affect the other is also a subject of interest.

Bibliography

[1] Pérez-Sánchez M, Sánchez-Romero F, Ramos H, López-Jiménez P. ”Modeling irrigation networks for the quantification of potential energy recovering: a case study”. Water/8:1–26/2016. http://dx.doi.org/10.3390/w8060234.

[2] Rossi M, Righetti M, Renzi M. Pump-as-turbine for energy recovery applications: the case study of an aqueduct. Energy Procedia 2016;101:1207–14. https://doi.org/10.1016/j.egypro.2016.11.163

[3] Carravetta A, Derakhshan S, Ramos HM. Pumps as Turbines Fundamentals and Applications. Springer International Publishing; 2018. https://doi.org/10.1007/978-3-319-67507-7.

[4] de Oliveira e Silva G, Hendrick P. Pumped hydro energy storage in buildings. Applied Energy 2016;179:1242–50. doi: https://doi.org/10.1016/j.apenergy.2016.07.046

[5] B. Capelo. Energy Recovery in Water Distribution Systems by a Pump Running as Turbine (PAT) – Grid Isolated Case. Master thesis, Instituto Superior Técnico, May 2017.

[6] A. A. Williams, N. P. Smith, C. Bird, and M. Howard. Pumps as turbines and induction motors as generators for energy recovery in water supply systems. Water and Environment Journal, 12(3): 175–178, 1998. doi: https://doi.org/10.1111/j.1747-6593.1998.tb00169.x

[7] B. Capelo, M. Pérez-Sánchez, J. F. Fernandes, H. M. Ramos, P. A. López-Jiménez, and P. J. Branco. Electrical behaviour of the pump working as turbine in off grid operation. *Applied Energy*, 208(September):302–311, 2017. https://doi.org/10.1016/j.apenergy.2017.10.039.

[8] J. F. P. Fernandes, M. Pérez-Sánchez, F. F. Silva, P. A. López-Jiménez, H. M. Ramos, and P. J. C. Branco. Optimal energy efficiency of isolated PAT systems by SEIG excitation tuning. *Energy Conversion and Management*, 183(January):391–405, 2019. https://doi.org/10.1016/j.enconman.2019.01.016.

[9] M. Pagaimo, Pumps as turbines (PATs): Series and parallel connections. Master thesis, Instituto Superior Técnico, November 2019.

[10] T. H. Phuong, MATLAB/Simulink Implementation and Analysis of Three Pulse-Width-Modulation (PWM) Techniques. Master thesis, Boise State University, May 2012.

[11] A. Dötlinger, R. Kennel, J. Stumper Loss Minimization of Induction Machines in Dynamic Operation *IEEE Transactions on Energy Conversion*, 28 (September): 726 - 735, 2013. doi: https://doi.org/10.1109/TEC.2013.2262048

[12] Khoury. G, Ghosn R., Khatounian F., Fadel M., Tientcheu M. Including Core Losses in Induction Motors Dynamic Model. 2016 3rd International Conference on Renewable Energies for Developing Countries, Zouk Mosbeh, Lebanon. doi: https://doi.org/10.1109/REDEC.2016.7577556

[13] S. D. Fitzgerald, A.E., Kingsley, Charles Jr., Umas. Electric machinery, volume 319. 2003. ISBN 0073660094. doi: 10.1016/0016-0032(85)90014-6.